Article

NMR-Based Analysis of Aminoglycoside Recognition by the Resistance Enzyme ANT(4#): The Pattern of OH/NH Substitution Determines the Preferred Antibiotic Binding Mode and Is Critical for Drug Inactivation

Julia Revuelta, Tatiana Vacas, Mario Torrado, Francisco Corzana, Carlos Gonzalez, Jesús Jiménez-Barbero, Margarita Menendez, Agatha Bastida, and Juan Luis Asensio

J. Am. Chem. Soc., **2008**, 130 (15), 5086-5103 • DOI: 10.1021/ja076835s • Publication Date (Web): 26 March 2008

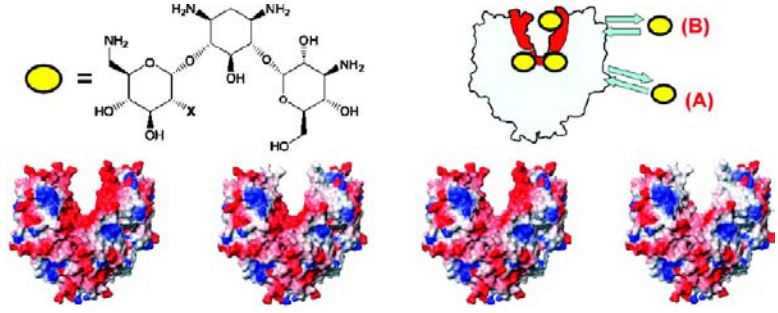

J|A|C|S
ARTICLES

Published on Web 03/26/2008

NMR-Based Analysis of Aminoglycoside Recognition by the Resistance Enzyme ANT(4′): The Pattern of OH/NH_3^+ Substitution Determines the Preferred Antibiotic Binding Mode and Is Critical for Drug Inactivation

Julia Revuelta,[†] Tatiana Vacas,[†] Mario Torrado,[†] Francisco Corzana,[‡] Carlos Gonzalez,[§] Jesús Jiménez-Barbero,[||] Margarita Menendez,[§] Agatha Bastida,*[,†] and Juan Luis Asensio*[,†]

Instituto de Química Orgánica General (CSIC), Madrid 28006, Spain, Departamento de Química, Universidad de La Rioja, UA-CSIC, Logroño 26006, Spain, Instituto de Química Física Rocasolano (CSIC) and Ciber Enfermedades Respiratorias, Madrid 28006, Spain, and Centro de Investigaciones Biológicas (CSIC), Madrid 28040, Spain

Received September 10, 2007; E-mail: iqoa110@iqog.csic.es

Abstract: The most significant mechanism of bacterial resistance to aminoglycosides is the enzymatic inactivation of the drug. Herein, we analyze several key aspects of the aminoglycoside recognition by the resistance enzyme ANT(4′) from *Staphylococcus aureus*, employing NMR complemented with site-directed mutagenesis experiments and measurements of the enzymatic activity on newly synthesized kanamycin derivatives. From a methodological perspective, this analysis provides the first example reported for the use of transferred NOE (trNOE) experiments in the analysis of complex molecular recognition processes, characterized by the existence of simultaneous binding events of the ligand to different regions of a protein receptor. The obtained results show that, in favorable cases, these overlapping binding processes can be isolated employing site-directed mutagenesis and then independently analyzed. From a molecular recognition perspective, this work conclusively shows that the enzyme ANT(4′) displays a wide tolerance to conformational variations in the drug. Thus, according to the NMR data, kanamycin-A I/II linkage exhibits an unusual anti-Ψ orientation in the ternary complex, which is in qualitative agreement with the previously reported crystallographic complex. In contrast, closely related, kanamycin-B is recognized by the enzyme in the syn-type arrangement for both glycosidic bonds. This observation together with the enzymatic activity displayed by ANT(4′) against several synthetic kanamycin derivatives strongly suggests that the spatial distribution of positive charges within the aminoglycoside scaffold is the key feature that governs its preferred binding mode to the protein catalytic region and also the regioselectivity of the adenylation reaction. In contrast, the global shape of the antibiotic does not seem to be a critical factor. This feature represents a qualitative difference between the target A-site RNA and the resistance enzyme ANT(4′) as aminoglycoside receptors.

Introduction

Aminoglycosides are a class of broad spectrum antimicrobial agents originally isolated from soil bacteria.[1–5] This group of antibiotics is important because they are often used to treat hospital-acquired infections caused by Gram-negative bacteria. Their primary target is the small ribosomal subunit. More specifically, aminoglycosides interact with the A-site decoding region of the 16S-rRNA, affecting the translation process by causing codon misreading or hindering the translocation step.[6–8]

Several years after the introduction of aminoglycosides in human antibacterial chemotherapy, resistant organisms began to appear. Indeed, the emergence of bacterial resistance to the major classes of antibiotics has become a major concern for the medical community.[9–13] Thus, there are examples of bacterial

[†] Instituto de Química Orgánica General (CSIC).
[‡] Universidad de La Rioja.
[§] Instituto de Química Física Rocasolano (CSIC).
[||] Centro de Investigaciones Biológicas (CSIC).

(1) Greenwood, D. In *Antimicrobial Chemotherapy*; Greenwood, D. Ed.; Oxford University Press: Oxford, 1995; pp 32–48.
(2) Walter, F.; Vicens, Q.; Westhof, E. *Curr. Opin. Chem. Biol.* **1999**, *3*, 694–704.
(3) Hermann, T. *Angew. Chem., Int. Ed.* **2000**, *39*, 1890–1905.
(4) Schroeder, R.; Waldsich, C.; Wank, H. *EMBO J.* **2000**, *19*, 1–9.
(5) Sucheck, J. S.; Wong, C. H. *Curr. Opin. Chem. Biol.* **2000**, *4*, 678–686.
(6) Carter, A. P.; Clemons, W. M.; Brodersen, D. E.; Morgan-Warren, R. J.; Wimberly, B. T.; Ramakrishnan, V. *Nature* **2000**, *407*, 340–348.
(7) (a) Vicens, Q.; Westhof, E. *Structure* **2001**, *9*, 647–658. (b) Vicens, Q; Westhof, E. *Chem. Biol.* **2002**, *9*, 747–755. (c) Francois, B.; Rusell, R. J. M.; Murray, J. B.; Aboul-ela, F.; Masquida, B.; Vicens, Q.; Westhof, E. *Nucleic Acids Res.* **2005**, *33*, 5677–5690.
(8) (a) Yoshizawa, S.; Fourmy, D.; Puglisi, J. D. *EMBO J.* **1998**, *17* (22), 6437–6448. (b) Fourmy, D.; Recht, M. I.; Blanchard, A. C.; Puglisi, J. D. *Science* **1996**, *274*, 1367–1371. (c) Lynch, S. R.; Gonzalez, R. L., Jr.; Puglisi, J. D. *Structure* **2003**, *11*, 43–53.
(9) Magnet, S.; Blanchard, J. *Chem. Rev.* **2005**, *105*, 477–497.
(10) Smith, C. A.; Baker, E. N. *Curr. Drug Targets* **2002**, *2*, 143–160.

10.1021/ja076835s CCC: $40.75

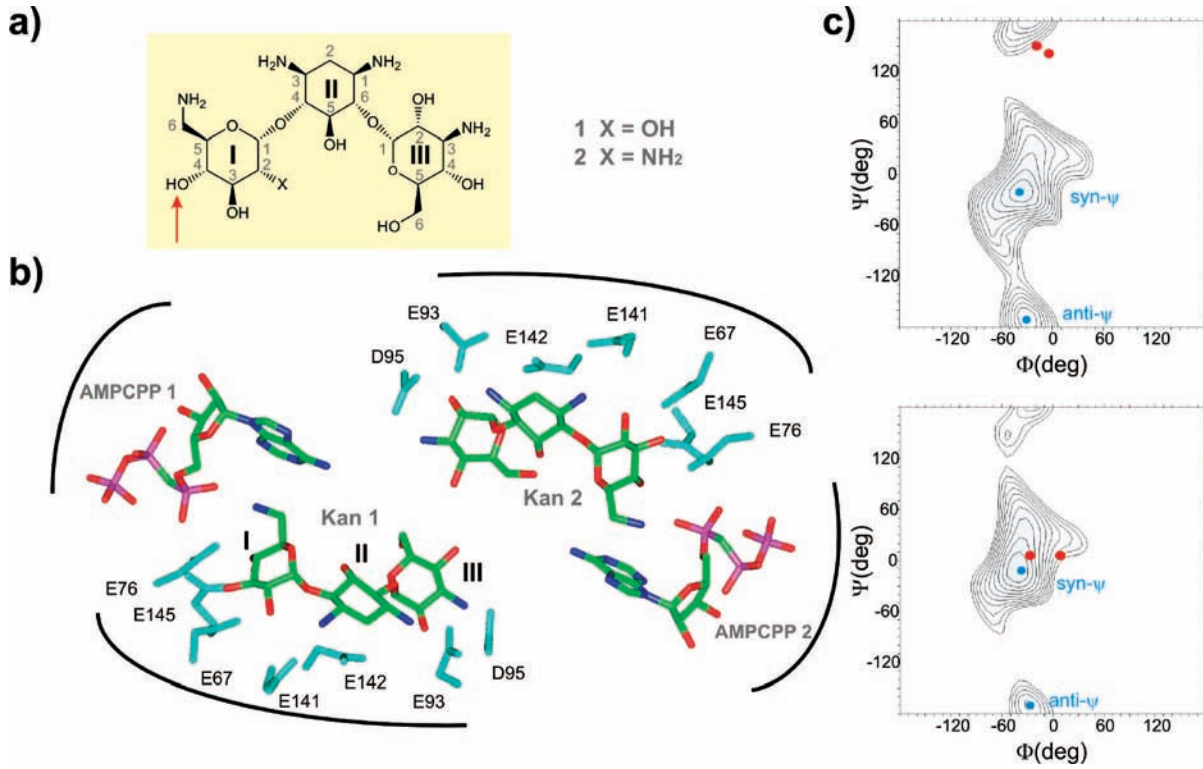

Figure 1. (a) Schematic representation of kanamycin-A (**1**) and B (**2**), together with the numbering employed for the different sugar units throughout the manuscript. The antibiotic position modified by the enzyme is indicated with an arrow. (b) X-ray structure of the ANT(4′)/kanamycin-A/AMPCPP ternary complex. Two antibiotic binding sites (one per monomer) are located at contiguous positions, close to the dimerization interface. Seven glutamate/aspartate side chains per monomer participate in direct contacts with the antibiotic. (c) Φ(H1−C1−O1−Cx)/Ψ(C1−O1−Cx−Hx) potential energy surfaces calculated with the AMBER* forcefield (see Supporting Information Figures S3−S4 for a more detailed conformational analysis) for kanamycin-A I/II (top) and III/II (bottom) glycosidic linkages. The location of the syn-Ψ/anti-Ψ minima are indicated by the blue circles. Φ/Ψ values observed for kanamycin-A in the crystallographic complex are shown with red circles. Level contours are given every 0.5 kcal/mol.

isolates insensitive to almost every antibacterial compound on the market, including several bacteria that cause life-threatening illnesses. Acquired resistance to aminoglycoside antibiotics can occur via three different mechanisms: mutation of the ribosomal target, reduced permeability for the antibiotics, and enzymatic modification of the drugs, thus leading to inactivation. However, from a clinical point of view, the most relevant source of resistance is conferred by the third mechanism, the enzymatic inactivation of the drugs.[9–13] Enzymes involved in bacterial defense against aminoglycoside antibiotics can be broadly classified as *N*-acetyltransferases (AACs), *O*-adenyl transferases (ANTs) and *O*-phosphotransferases (APHs). These antibiotic modifying enzymes (AME) are primary pharmacological targets. It is evident that the structural analysis of these proteins in complex with the drugs could provide valuable information for the design either of novel aminoglycosides, not susceptible to modification, or of enzymatic inhibitors. Indeed, the development of new strategies to overcome bacterial resistance constitutes an active field of research.[14–20]

Herein, we analyze several key aspects of the aminoglycoside recognition by the resistance enzyme ANT(4′) from *Staphylococcus aureus* using a NMR-based approach. ANT(4′) is one of the main representatives of the nucleotidyltransferases family of AMEs. It catalyzes the transfer of one adenyl group from ATP to position O-4 (Figure 1) of the glucose unit (ring I), present in most aminoglycosides. This transfer leads to a sharp decrease in the drug affinity for its target RNA. The 3D structure of the antibiotic in the ternary complex ANT(4′)/kanamycin-A (**1**)/AMPCPP (a nonhydrolyzable ATP analogue) has been described by X-ray methods.[21]

According to these data, ANT(4′) forms a dimeric structure of 66 kD. The kanamycin-A binding sites (one per monomer), located close to the dimerization interface, are characterized by

(11) Azucena, E.; Mobashery, S. *Drug Resistance Updates* **2001**, *4*, 106–117.
(12) Jana, S.; Deb, J. K. *Appl. Microbiol. Biotechnol.* **2006**, *70*, 140–150.
(13) Wright,G. D. In *Bacterial Resistance to Antimicrobials*; Lewis, K., Salyers, A. A., Taber, H. W., Wax, R. G., Eds.; Marcel Dekker: New York, 2002; pp 91–121.
(14) Zhou, J.; Wang, G.; Zhang, L.; Ye, X. *Med. Res. Rev.* **2006**, 1–38.
(15) (a) Kondo, S.; Iinuma, K.; Yamamoto, H.; Maeda, K.; Umezawa, H. *J. Antibiot.* **1975**, *26*, 412–417. (b) Kondo, S.; Hotta, K. *J. Infect. Chemother.* **1999**, *5*, 1.
(16) Inoue, M.; Nonoyama, M.; Okamoto, R.; Ida, T. *Drugs Exp. Clin. Res.* **1994**, *20*, 233–239.
(17) Fujimura, S.; Tokue, Y.; Takahashi, H.; Nukiwa, T.; Hisamichi, K.; Mikami, T.; Watanabe, A. *J. Antimicrob. Chemother.* **1998**, *41*, 495–499.
(18) (a) Roestamadji, J.; Graspas, I.; Mobashery, S. *J. Am. Chem. Soc.* **1995**, *117*, 11060–11069. (b) McKay, G. A.; Roestamadji, J.; Mobashery, S.; Wright, G. D. *Antimicrob. Agents Chemother.* **1996**, *40*, 2648–2650. (c) Haddad, J.; Vakulenko, S.; Mobashery, S. *J. Am. Chem. Soc.* **1999**, *121*, 11922–11923. (d) Grapsas, I.; Lerner, S. A.; Mobashery, S. *Arch. Pharm.* **2001**, *334*, 295–301.
(19) (a) Bastida, A.; Hidalgo, A.; Chiara, J. L.; Torrado, M.; Corzana, F.; Cañadillas, J. M.; Groves, P.; Garcia-Junceda, E.; Gonzalez, C.; Jimenez-Barbero, J.; Asensio, J. L. *J. Am. Chem. Soc.* **2006**, *128*, 100–116. (b) Asensio, J. L.; Hidalgo, A.; Bastida, A.; Torrado, M.; Corzana, F.; Junceda, E. G.; Canada, J.; Chiara, J. L.; Jiménez-Barbero, J. *J. Am. Chem. Soc.* **2005**, *127*, 8278–8279.
(20) Hanessian, S.; Szychowsky, J.; Campos-Reales, N. B.; Furtos, A.; Keillor, J. W. *Bioorg. Med. Chem. Lett.* **2007**, *17*, 3221–3225.
(21) Pedersen, L. C.; Benning, M. M.; Holden, H. M. *Biochemistry* **1995**, *34*, 13305–13311.

the presence of up to seven acid residues per monomer, involved in antibiotic recognition. Regarding the aminoglycoside structure, the crystallographic data show that the enzyme selects high-energy conformations (Figure 1) of the drug. In particular, the I/II fragment of the saccharide adopts a distorted geometry (Φ/Ψ values –4°/142° and –21°/152°) located out of the syn-Ψ or anti-Ψ low energy regions, present on the potential energy surfaces (see Figures 1, S3, and S4) calculated with either AMBER* or MM3* force-fields. These deviations represent significant energy penalties (estimated energy differences with respect to the syn-Ψ and anti-Ψ minimum energy geometries for the two kanamycin molecules present in the crystallographic complex are $\Delta E_{\text{Xray/syn-}\Psi} = 4.7/7.4$ kcal/mol and $\Delta E_{\text{Xray/anti-}\Psi} = 3.5/6.2$ kcal/mol, according to AMBER*, and $\Delta E_{\text{Xray/syn-}\Psi} = 6.4/9.0$ kcal/mol and $\Delta E_{\text{Xray/anti-}\Psi} = 3.6/6.2$ kcal/mol, according to MM3* calculations). Moreover, the kanamycin-A conformations observed in the crystallographic complex are also significantly different to those reported for free antibiotic by X-ray methods ($\Phi/\Psi = -18.4°/-1.2°$).[22] High energy or distorted conformations have been observed in different complexes for other carbohydrates and, in several occasions, these distortions seem to have a clear functional relevance. In fact, it has been shown that they are not unusual if the oligosaccharides incorporate scissile bonds.[23] However, the I/II linkage in kanamycin-A is not broken by the action of ANT(4′) and therefore the functional relevance of the high energy geometry observed for the antibiotic is, at the moment, unclear. Interestingly, recent studies, employing conformationally constrained aminoglycoside derivatives, strongly suggest that the enzyme must be able to recognize and, thus, inactivate different conformations of the antibiotic.[19a] This particular point is of key relevance for the design of inhibitors or new drugs nonsusceptible to enzymatic inactivation. In addition, previous studies have shown that ANT(4′) selectively modifies position 4 of ring I in kanamycin-A (**1**).[24] However, given the electrostatic nature of the recognition process and the apparent symmetry of kanamycin-A, the regioselectivity exhibited by the enzyme seems surprising. To determine the conformational requirements of aminoglycoside inactivation by ANT(4′) and to clarify the structural basis for the enzyme regioselectivity, we have performed a detailed NMR-based analysis of the molecular recognition process underlying catalysis. As a first step, we have analyzed the conformational properties of kanamycin-A (**1**) and B (**2**) in the protein-bound state employing transferred NOE experiments (trNOE) on both, wild-type and mutated enzymes. These studies were complemented by measurements of the enzymatic activity on designed derivatives.

TrNOE experiments are nowadays frequently used to analyze the conformation of different ligands bound to medically relevant receptors or enzymes.[25–27] However, it should be emphasized that, given the electrostatic nature of the protein/ligand interaction and inherent complexity of the binding processes, the NMR analysis of the ANT(4′)/aminoglycoside recognition is a challenging task. A general limitation in the application of NMR to analyze molecular recognition processes arises from the existence of simultaneous binding events of the ligand to different regions of the receptor. Under these circumstances, all of them might contribute to the observed intraligand trNOE cross-peaks. Unfortunately, these different contributions can not be separated in a simple way and the interpretation of the NMR data in terms of a single binding mode can lead to erroneous conclusions. The coexistence of different binding processes is quite extended in biological systems, especially in those cases where both the ligand and the receptor are highly charged species. ANT(4′) provides a clear example of this situation. Herein we show that, in favorable cases, these different binding events can be isolated through site-directed mutagenesis following a protocol that may also be of applicability to dissect specific from nonspecific binding in other relevant biomedical and biological systems. This study provides a key example of how trNOE measurements can be applied to derive the protein-bound conformation of low molecular weight ligands in highly charged systems and shows that, in these cases, the possibility of simultaneous binding of the ligand to different regions of the receptor must be carefully considered.

From a molecular recognition perspective, the obtained results provide genuine insights into different aspects of the aminoglycoside recognition and inactivation by ANT(4′). Thus, we have shown that binding of kanamycin-A (**1**) to the catalytic region of ANT(4′) (herein referred as region A) causes a significant increase in the internal mobility of the glycoside I/II linkage. In presence of both ATP/Ca^{2+} or AMPCPP/Mg^{2+} (ternary complexes) the protein selects a single conformation of the drug. This geometry is well within the low energy anti-Ψ region predicted by both AMBER* and MM3* calculations and presents similarities with those observed in the crystallographic complex. However, both structures are not identical. Thus, for the I/II linkage, differences in the aglyconic Ψ angle amount to 41°/51°. Interestingly, although kanamycin-A and kanamycin-B share an identical covalent scaffold (in fact, they differ in a single position) they adopt a totally different conformation in the enzyme catalytic region, according to the trNOE data. This result indicates that the spatial charge distribution of the aminoglycoside is the key feature that determines its geometrical features in the bound state and shows that ANT(4′) exhibits a significant tolerance to conformational variations of the drug. Finally, the analysis of the enzymatic inactivation of several non-natural kanamycin derivatives indicates that the antibiotic

(22) (a) Puius, Y. A.; Stievater, T. H.; Srikrishnan, T. *Carbohydr. Res.* **2006**, *341*, 2871–2875. (b) Koyama, G.; Iitaka, Y.; Maeda, K.; Umezawa, H. *Tetrahedron Lett.* **1968**, *15*, 1875–1878.
(23) French, A. D.; Johnson, G. P.; Kelterer, A. M.; Dowd, M. K.; Cramer, C. J. *Int. J. Quantum Chem.* **2001**, *84*, 416–425.
(24) Gerratana, B.; Cleland, W. W.; Reinhardt, L. A. *Biochemistry* **2001**, *40*, 2964–2971.
(25) (a) Angulo, J.; Langpap, B.; Blume, A.; Biet, T.; Meyer, B.; Krishna, N. R.; Peters, H.; Palcic, M. M.; Peters, T. *J. Am. Chem. Soc.* **2006**, *128*, 13529–13538. (b) Haselhorst, T.; Weimar, T.; Peters, T. *J. Am. Chem. Soc.* **2001**, *123*, 10705–10714. (c) Haselhorst, T.; Espinosa, J. F.; Jiménez-Barbero, J.; Sokolowski, T.; Kosma, P.; Brade, H.; Brade, L.; Peters, T. *Biochemistry* **1999**, *38*, 6449–6459. (d) Scheffler, K.; Ernst, B.; Katopodis, A.; Mignani, J. L.; Wang, W. T.; Weisemann, R.; Peters, T. *Angew. Chem., Int. Ed. Engl.* **1995**, *34*, 1841–1844.
(26) (a) Owston, M. A.; Serpersu, E. H. *Biochemistry* **2002**, *41*, 10764–10770. (b) DiGiammarino, E. L.; Draker, K.; Wright, G. D.; Serpersu, E. H. *Biochemistry* **1998**, *37*, 3638–3644. (c) Cox, J. R.; Serpersu, E. H. *Biochemistry* **1997**, *36*, 2353–2359.
(27) (a) Corzana, F.; Cuesta, I.; Bastida, A.; Hidalgo, A.; Latorre, M.; González, C.; García-Junceda, E.; Jiménez-Barbero, J.; Asensio, J. L. *Chem. Eur. J.* **2005**, *11*, 5102–5113. (b) Espinosa, J. F.; Cañada, J.; Asensio, J. L.; Dietrich, H.; Martín-Lomas, M.; Schmidt, R. R.; Jiménez-Barbero, J. *Angew. Chem., Int. Ed. Engl.* **1996**, *35*, 303–306.; *Angew. Chem.* **1996**, *108*, 323–326. (c) Espinosa, J. F.; Montero, E.; Vian, A.; Garcia, J.; Dietrich, H.; Martín-Lomas, M.; Schmidt, R. R.; Imberty, A.; Cañada, J.; Jiménez-Barbero, J. *J. Am. Chem. Soc.* **1998**, *120*, 10862–10871. (d) Garcia, A.; Montero, E.; Muñoz, J. L.; Espinosa, J. F.; Vian, A.; Asensio, J. L.; Cañada, F. J.; Jimenez-Barbero, J. *J. Am. Chem. Soc.* **2002**, *124*, 4804–4810.

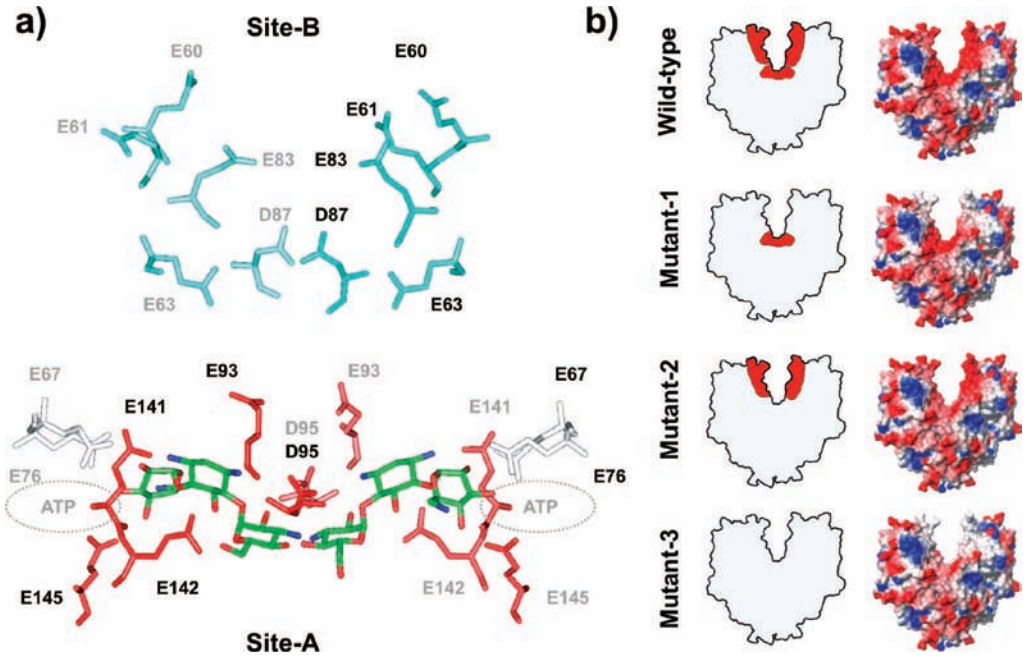

Figure 2. (a) Schematic representation of aspartate and glutamate side chains located at sites A and B. The structural data suggest that the antibiotic might have independent access to both sites A and B (that is, in order to bind to site A the drug would not have to go necessarily through site B). Residues in cyan have been replaced in mutant-1. Residues in red have been replaced in mutant-2. Both type of residues have been substituted in mutant-3. The location of the ATP in the catalytic region A is also indicated. (b) Schematic representation of the wild-type and mutated proteins, together with the corresponding electrostatic potential.

charge distribution is also at the origin of the regioselectivity exhibited by the adenylation reaction.

Results and Discussion

Isolating Different Binding Events through Site Directed Mutagenesis. Given the intrinsic features of this system, for which complexation is mainly driven by electrostatic forces, the possibility of simultaneous binding of the antibiotic to different protein regions must be carefully considered. For ANT(4′) close inspection of the protein charge distribution reveals an additional potential site for binding of aminoglycosides (labeled as B in Figure 2a), located close to the primary binding region detected in the crystal (labeled as A in Figure 2a). This putative binding region is constituted by a narrow funnel lined with up to ten glutamate/aspartate side chains (five per monomer).

To confirm this hypothesis and to separate the two binding processes, three variants of the wild-type protein were designed and produced by site directed mutagenesis. First, the putative aminoglycoside binding site (B) was removed employing five conservative substitutions (mutant-1 in Figures 2b and S1): E60Q, E61Q, E63Q, E83Q, and D87N. In addition, the binding region (A), identified in the crystallographic complex, was removed by the E93Q, D95N, E141Q, E142Q, and E145Q mutations (mutant-2 in Figures 2b and S1). Finally, both binding sites (A and the putative site B) were simultaneously removed from the enzyme by the ten substitutions (mutant-3 in Figures 2b and S1).

ANT(4′) variants 1–3 were obtained, expressed, and purified as described in the Materials and Methods section. Several controls were performed in order to warrant the structural integrity of the obtained proteins. First, analytical ultracentrifugation measurements showed that all of them are dimeric up to 0.5 μM concentration (MW 66 kDa, which is indicative of dimerization constants in the submicromolar range). Second,

Table 1. Apparent Kinetic Parameters Estimated for Kanamycin-A and B and All the Enzyme Variants in 20 mM Phosphate at pH 7.5[a]

		wild-type	mutant-1	mutant-2	mutant-3
kan-A (1)	k_{cat}	0.06 ± 0.01	0.12 ± 0.02	0.0002 ± 0.0001	nd
	K_m	0.03 ± 0.01	0.04 ± 0.01	nd	nd
kan-B (2)	k_{cat}	0.33 ± 0.04	0.44 ± 0.05	0.0006 ± 0.0001	nd
	K_m	0.09 ± 0.01	0.09 ± 0.01	nd	nd

[a] K_m and k_{cat} values are given in mM and s^{-1} units, respectively. The reported values are an average of three independent experiments. Nd stands for "not determined".

the far UV CD spectra measured for the mutated enzymes are consistent with similar secondary structure contents to that exhibited by the wild-type protein. In addition, according to CD melting profiles, mutant-3 has a thermal stability identical to that observed for the wild-type protein, while mutants 1 and 2 are marginally less stable (T_m = 328.5 K for wild-type ANT(4′), 327.1 K for mutant-1, 325.4 K for mutant-2, and 328.2 K for mutant-3, Figure S2). As a third control, the nucleotidyltransferase activity of the three variants was measured against both kanamycin-A (**1**) and kanamycin-B (**2**). These assays showed that mutant-1 is slightly more active than the wild-type protein (Table 1). In contrast, for mutants 2 and 3 kanamycin-A adenylation was detected only after several hours at very high protein concentration (>20 μM). This result was expected as those residues involved in aminoglycoside binding at the enzyme catalytic center (site A) have been substituted by the mutations, including E145, proposed to act as general base in the catalysis from the X-ray data.[21,24,28,29]

Finally, a preliminary characterization of the aminoglycoside binding properties exhibited by the wild type and mutated

(28) Chen-Goodspeed, M.; Vanhooke, J. L.; Holden, H. M.; Raushel, F. M. *Bioorg. Chem.* **1999**, *27*, 395–408.
(29) Gerratana, B.; Frey, P. A.; Cleland, W. W. *Biochemistry* **2001**, *40*, 2972–2977.

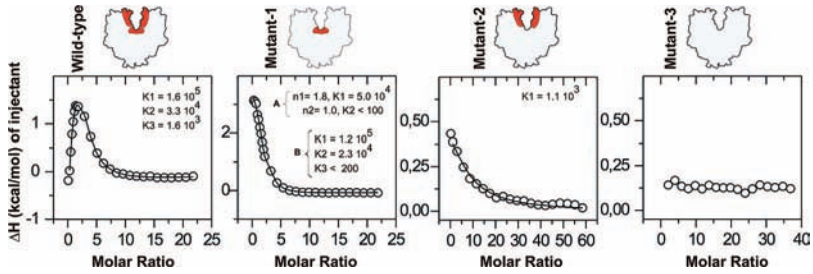

Figure 3. ITC profiles for the titration of kanamycin-A into solutions containing wild-type ANT(4′) and mutants 1–3 at 25 °C and pH 7.0 in 10 mM phosphate. The solid line represents the least-squares fitting of the data to the simplest model compatible, in each case (see the Materials and Methods section). For the wild-type protein fitting was performed assuming three sequential binding sites per dimer. For mutant-1, two sets of binding sites (model A) or three sequential binding sites (model B) per dimer were considered. For mutant-2 data were fitted assuming a single site. Estimated K_b values are indicated.

proteins (binary complexes) was performed employing isothermal titration microcalorimetry (ITC). Thermal titration curves (Figures 3, S5−S8) conclusively show that the mutations significantly affect the protein/antibiotic interactions. Thus, the analysis of the binding curves for the wild-type ANT(4′) and the mutant 1 are consistent with the tight complexation of two molecules of kanamicin-A per protein dimer (presumably reflecting the interaction of the antibiotic with the catalytic region A). However, binding sites are not equivalent in the wild-type enzyme and the theoretical fitting in terms of the simplest model, compatible with the experimental data (three sequential sites per protein dimer; see Materials and Methods section), shows that complexation of the first kanamycin-A molecule is slightly endothermic ($\Delta H_b^1 = 0.4$ kcal/mol) while the second one binds with a positive enthalpy value ($\Delta H_b^2 = 4.3$ kcal/mol). Additional medium-low affinity binding (K_b^3 in the 10^3 M^{-1} range) could result from interactions of the aminoglycoside with the highly charged site-B.

For mutant 1, the two high affinity sites per dimer detected behave as equivalent and the binding curve can be described in terms of two sets of sites. Thus, binding to the high affinity sites ($n_1 = 1.8$, $K_b = 5.0 \times 10^4$ M^{-1}) is clearly endothermic ($\Delta H_b = 4.6$ kcal/mol). A very weak binding process ($K_b < 100$ M^{-1}) has also to be considered to fit the experimental curves, probably reflecting unspecific electrostatic interactions between the enzyme and the aminoglycoside. For comparison purposes, the titration curves of mutant 1 were also analyzed assuming three sequential sites per protein dimer. This analysis yielded two high affinity sites whose binding constants differ by a factor of about 4, (as expected for equivalent and independent sites).[30] The derived *K*b values (see Figure 3) are comparable to those measured for the wild-type protein but, in contrast with the behavior exhibited by this enzyme, for mutant-1, the two binding processes present similar enthalpies ($\Delta H_b^1 = 3.5$ and $\Delta H_b^2 = 3.9$ kcal/mol).

Regarding variant-2, in which charges from site A have been removed, the titration curves conclusively show that it retains a certain aminoglycoside binding activity (K_b values in the 10^3 M^{-1} range). Unfortunately, the complex stoichiometry cannot be determined under the employed experimental conditions (available protein concentration is limited by the protein solubility). Despite the relatively low affinity for kanamcin-A exhibited by site B, aminoglycoside binding to this protein region could certainly be relevant from a NMR perspective. In fact, medium-low affinity complexes, like this, are usually considered optimal for the measurement of trNOEs (tight binding is characterized by lower off rate, k_{-1}, constants and tends to produce low intensity trNOE cross peaks)

Finally, no complex formation was detected for mutant-3.

The experimental binding enthalpies for wild-type ANT(4′) and mutants 1–2 show a significant variation with the pH (see Figures S6−S7). Thus, at pH 7.8 the binding process is clearly exothermic. Although merely speculative, this behavior is likely to reflect, at least partially, the binding-coupled protonation of the aminoglycoside. On the other hand, deprotonation of kanamicin-A above neutrality would result in a reduction of the apparent binding constants as the pH increases, which is in contrast with the obtained experimental data (Figures S6−S7) and suggests that the antibiotic complexation might also involve the specific ionization of certain aspartic/glutamic acid side chains in the enzyme.

Previous studies have shown that binding of aminoglycosides to resistance enzymes or RNA is usually linked to the protonation of specific amino groups of the drug in a pH dependent manner.[31–33] Indeed, a similar behavior, with ΔH_b values strongly exothermic at basic pH and close to 0 or even endothermic at neutral or slightly acid pH values, has been reported for the interaction between neomycin-B and the A-site RNA.[31] The linkage between binding and protonation has a large influence on the binding thermodynamics. Indeed, under these circumstances, the experimental enthalpies could include significant contributions arising from de/protonation of the drug amino groups or the protein as well as from the buffer ionization. Taking this into account, minor differences in the pK_a of specific protein side chains might be at the origin of the subtle enthalpic differences between the wild-type enzyme and mutant 1, revealed by the ITC data. In fact, these contributions might differ for the different mutants, which preclude a further interpretation of the experimental ΔH_b values in terms of the specific protein/aminoglycoside interactions established within the complexes without a more detailed thermodynamic analysis.

NMR Analysis of Kanamycin-A Conformational Features in the Protein-Bound State: Preliminary Considerations. As a first test, trNOE experiments were performed employing

(30) Wyman, J.; Gill, S. J. In *Binding and Linkage. Functional Chemistry of Biological Macromolecules;* University Science Books: Mill Valley, CA, 1990; 44–46.

(31) (a) Kaul, M.; Barbieri, C. M.; Kerrigan, J. E.; Pilch, D. S. *J. Mol. Biol.* **2003**, *326*, 1373–1387. (b) Kaul, M.; Pilch, D. S. *Biochemistry* **2002**, *41*, 7695–7706. (c) Barbieri, C. M.; Pilch, D. S. *Biophys. J.* **2006**, *90*, 1338–1349.

(32) Ozen, C.; Malek, J. M.; Serpersu, E. H. *J. Am. Chem. Soc.* **2006**, *128*, 15248–15254.

(33) Freire, F.; Cuesta, I.; Corzana, F.; Revuelta, J.; González, C.; Hricovini, M.; Bastida, A.; Jiménez-Barbero, J.; Asensio, J. L. *Chem. Commun.* **2007**, *2*, 174–176.

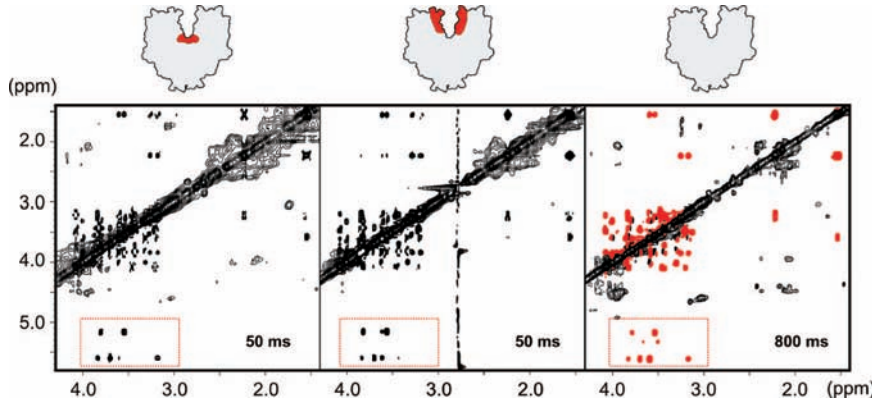

Figure 4. NOESY experiments measured for kanamycin-A (2.5 mM) in presence of 80 μM concentration of mutants 1, 2, and 3 (from left to right) in 10 mM phosphate, 5 mM $MgCl_2$, pH 7.8, and 303 K. For mutant-3, positive NOEs were obtained in all the conditions tested. The employed mixing time is also indicated.

compound **1** and the four ANT(4′) variants (wild-type and mutants 1–3).

For mutant-3, no trNOEs were detected under any experimental conditions, in agreement with the absence, in this protein, of the aminoglycoside binding regions, A and B (Figure 4). In all other cases, clear negative cross-peaks were measured, which provides further support for the assignment of B as a nonspecific binding site.

The highest quality NMR spectra were recorded at pH 7.8 (at neutral and acid pH values the protein solubility is significantly reduced). These pH conditions are close to those optimal for enzymatic activity, according to previous studies, and were employed throughout our work. [28]

To analyze the enzyme-bound antibiotic conformation, both in binary or ternary complexes (that is the absence or presence of ATP/Ca^{2+} or AMPCPP/Mg^{2+}), NOE build up curves were obtained from trNOESY experiments at different mixing times, and the apparent cross-relaxation rates were derived from the initial slopes (Figure S9). In addition, simulations of the trNOE build-up curves were performed employing the crystallographic data and assuming different geometries for the kanamycin-A bound state. The theoretical treatment of the trNOE data is essential to evaluate the influence of the spin diffusion on the measured cross-peaks (if spin diffusion is present, which is not unlikely for a complex of this size, this could dramatically alter the observed cross-relaxation rates, leading to erroneous conclusions). This analysis was performed with the program CORCEMA (complete relaxation and conformational exchange matrix)[34] that allows computation of NOEs (using a full relaxation matrix approach) for systems in chemical exchange.

To determine the conformational changes induced in the drug by the recognition process (and to evaluate the thermodynamic implications of these alterations) a previous understanding of the ligand conformational features in the free state is required. A detailed description of kanamycin-A (**1**) structure in solution has been recently reported by our group.[35] According to our results the antibiotic conformational behavior is extremely sensitive to the pH conditions. At pH 7.8, the I/II linkage exhibits two unequally populated orientations herein referred as syn-Ψ (Φ/Ψ –34°/−20°, around 80% population, characterized by a short H1−I/H4−II distance, see Figure 5a) and anti-Ψ (Φ/Ψ –30°/−167°, around 20% population, characterized by short H1−I/H3−II and H1−I/H5−II distances) minima (Figure 5a). These geometries correspond to local minima in the potential energy surface calculated for **1** by molecular mechanics (see Figure 1b). In contrast, for the III/II linkage, a unique syn-Ψ arrangement (Φ/Ψ –41°/−11°, characterized by a short H1−III/H6−II distance) was detected.

NMR Analysis of Kanamycin-A/ANT(4′) Binary Complex. Conformation of Kanamycin-A Bound to the Antibiotic Binding Site A. The conformational properties of **1** bound by the catalytic region A were first studied in the absence of Mg^{2+}, employing the ANT(4′) variant-1 (see Figure 2). Figure 5b (upper panel) shows a key region of a typical trNOESY spectrum, together with the structurally relevant NOE build-up curves. According to these data, the antibiotic II/III fragment remains rigid and exhibits an orientation nearly identical to that detected in the free state (as proved by the observed large H1−III/H6−II contact. See Figure 5 panels a and b for a comparison). A different behavior is observed for the I/II linkage. Thus, a clear increase in the relative intensities of the H1−I/H5−II and H1−I/H3−II cross-relaxation rates, representative of the anti-Ψ geometry, is evident in all cases. In fact, the key interresidue H1−I/H3−II and H1−I/H5−II contacts exhibit a slightly larger intensity than H1−I/H4−II in the trNOE experiments. The simultaneous occurrence of these NOEs is not compatible with any single low-energy geometry of the glycosidic linkage and strongly suggests the existence of a significant degree of internal mobility for the I/II antibiotic region. CORCEMA simulations provide a theoretical support for this conclusion showing that, at the employed ligand:protein ratio (30:1), the influence of spin diffusion mediated by the protein or by other ligand protons on the observed key cross peaks is negligible (Figure S10). This result might seem surprising given the large molecular weight of the antibiotic/enzyme complex. However, it should be kept in mind that, according to the X-ray data, the ligand does not present any close van der Waals contacts with hydrophobic or aromatic side chains of the enzyme, which strongly reduces the possibility of protein-mediated spin diffusion. This might be a general feature of those binding processes mainly driven by electrostatic forces and polar contacts.

In conclusion, the NMR data are indicative of a significant increase of the antibiotic conformational variability upon binding

(34) Lee, W.; Rama Krishna, N. *J. Magn. Reson.* **1992**, *98*, 36–48.

(35) Corzana, F.; Cuesta, I.; Freire, F.; Revuelta, J.; Torrado, M.; Bastida, A.; Jimenez-Barbero, J.; Asensio, J. L. *J. Am. Chem. Soc.* **2007**, *129*, 2849–2865.

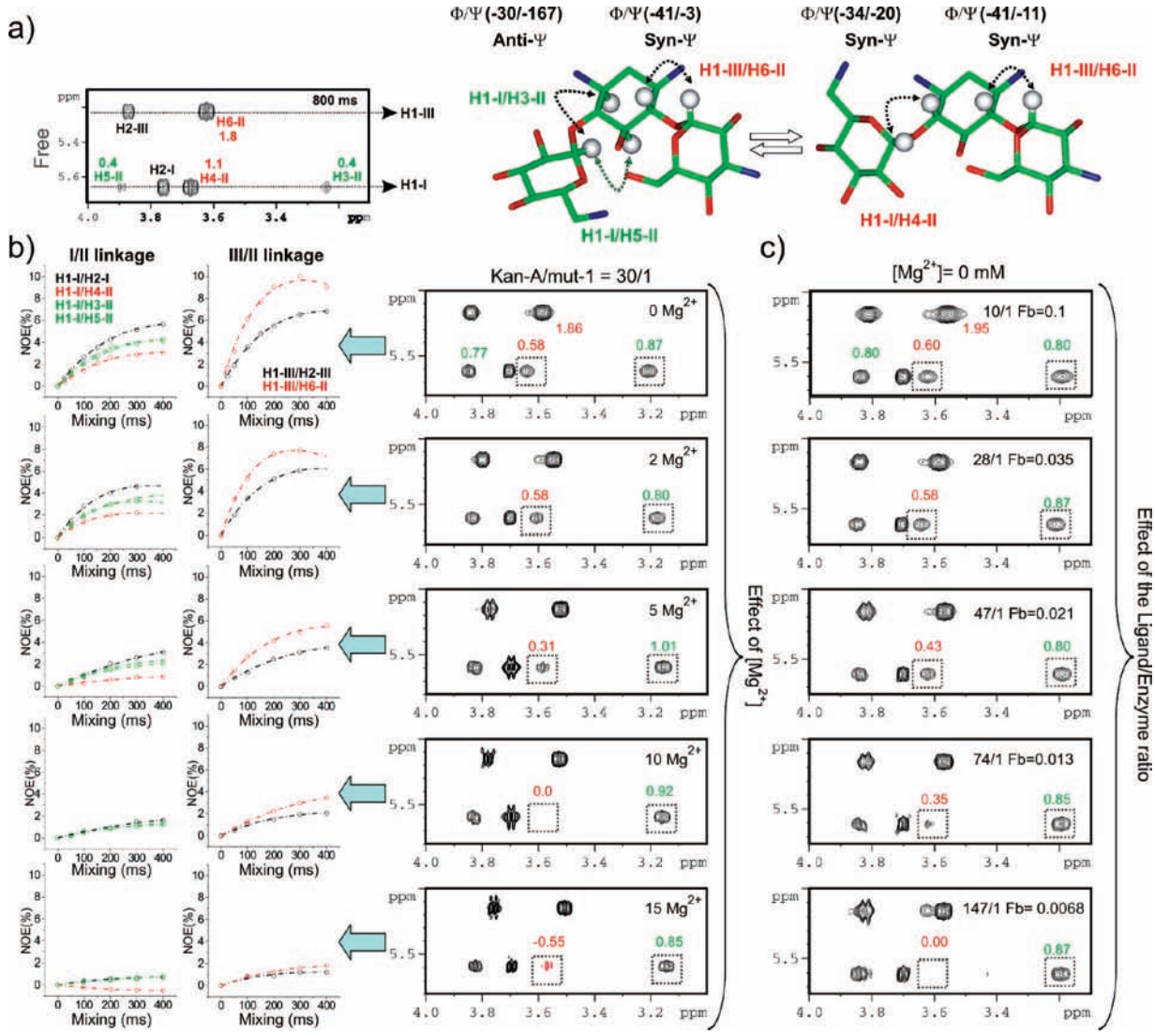

Figure 5. (a) (Left) NOESY spectrum measured for free kanamycin-A together with a representation of the syn-Ψ and anti-Ψ minimum energy geometries (right). NOEs representative of syn-Ψ and anti-Ψ minima are coloured in red and green, respectively. Experimental ratios between the structurally relevant cross relaxation rates and those corresponding to the known fixed distances, H1−I/H2−I and H1−III/H2−III, for units I and III, respectively, are indicated above the cross-peaks. (b) trNOESY (mixing 100 ms) spectra acquired in presence of mutant-1 at several Mg^{2+} concentrations. Structurally relevant NOE build-up curves are shown on the left. The effect of Mg^{2+} on the ratios $\sigma_{H1-I/H4-II}/\sigma_{H1-I/H2-I}$ and $\sigma_{H1-I/H3-II}/\sigma_{H1-I/H2-I}$ is highlighted. (c) trNOESY (mixing 100 ms) spectra acquired at different ligand/mutant-1 ratios without Mg^{2+}. The effect of the fraction of bound ligand (Fb) on $\sigma_{H1-I/H4-II}/\sigma_{H1-I/H2-I}$ and $\sigma_{H1-I/H3-II}/\sigma_{H1-I/H2-I}$ is also highlighted.

to protein site A. This fact could simply reflect the coexistence of different binding modes of the drug to the same protein region. However, even assuming multiple binding modes, the large internal variability detected for kanamycin-A is intriguing and deserves a further explanation. As previously mentioned, the conformational behavior of the antibiotic I/II linkage, in absence of the protein, is extremely sensitive to the pH conditions.

In fact, our previous studies have shown that at pH 4.0 (the fully protonated state of the drug), the I/II glycosidic linkage exhibits a remarkable flexibility, with syn-Ψ and anti-Ψ states equally populated.[35] Under these circumstances, the key inter-residue cross-peaks H1−I/H4−II, H1−I/H3−II and H1−I/H5−II present a nearly identical intensity (Figure S11). At higher pH values, the fraction of anti-Ψ geometries is gradually decreased from 50% at pH 4.0 to less than 20% at pH > 9.0. Interestingly, the trNOE data measured for the binary complex at pH 7.8 closely resemble the NOE data obtained for kanamycin-A (in the absence of the protein) at pH 4.0 (that is, in its fully protonated state, see Figure S11).

In our opinion, the highly dynamical conformational behavior exhibited by **1** in the bound state is likely to reflect, at least in part, the change in its protonation state upon binding to ANT(4′). This would be in agreement with previous studies on aminoglycoside recognition by both RNA or resistance enzymes.[31–33]

The coexistence of multiple conformations of the antibiotic in the protein/aminoglycoside binary complex is in contrast with the unique high-energy conformation of kanamycin-A observed in the crystallographic ternary complex and strongly suggests that the nucleotide three-phosphate might be essential to select a particular conformational state of the antibiotic.

Influence of Mg^{2+} on Kanamycin-A Binding to Mutant-1. Given that the formation of the ternary complex requires the presence of Mg^{2+}, the effect of this ion on the aminoglycoside/enzyme complex was also analyzed. Figure 5b shows typical spectra obtained for **1** in presence of mutant-1, at different Mg^{2+}

concentrations and identical pH conditions (pH 7.8). It can be observed that this ion causes a uniform reduction of the cross relaxation rates corresponding to the different cross peaks. In principle, this could simply reflect a decrease in the protein/aminoglycoside complex stability with the subsequent reduction in the molar fraction of bound antibiotic. This point was confirmed by ITC measurements (Figure S8) that clearly showed a sharp drop in binding affinity in the presence of this ion. Considering the highly charged nature of both, the aminoglycoside and the enzyme catalytic region A, the binding strength is expected to be extremely sensitive to the employed buffering conditions (pH and salt concentration). It is well established that, for such systems, screening of protein/ligand electrostatic interactions by salt, opposes binding. However, we would like to point out that, the influence of Mg^{2+} on the binding process cannot be explained by this effect alone. Thus, in comparison, NaCl at identical ionic strength, seem to have a much minor effect on kanamycin-A binding, according to both, ITC and trNOE data (see Figure S8). Although merely speculative, the most likely explanation for the observed behavior is that Mg^{2+} effectively competes with the drug for heavily charged aminoglycoside binding regions, A and B, present in the enzyme. Interestingly, at concentrations of Mg^{2+} larger than 2 mM the relative intensities of the different cross-peaks are also significantly altered. Thus, the ratio between the cross relaxation rates $\sigma_{H1-I/H4-II}/\sigma_{H1-I/H2-I}$ (the H1−I/H2−I cross peak corresponds to a fixed distance of 2.4 Å and was used as reference) varies from 0.58 in the absence of Mg^{2+} to –0.55 at 15 mM Mg^{2+}. It would be temping to interpret these changes in structural terms, concluding that the protein-bound conformation of kanamycin-A is sensitive to the presence of Mg^{2+}. However, it should be kept in mind that this ion causes an increase in the molar fraction of free kanamycin-A. At the exchange regime exhibited by the system (k_{-1} around 300 s^{-1} for mutant-1 in the absence of Mg^{2+} according to CORCEMA simulations) and the employed ligand: protein ratio (30:1), the contribution of free kanamycin-A to the average cross relaxation rates might be significant, affecting in different proportions the different cross peaks. To evaluate this possibility, trNOESY experiments were performed with mutant-1 in the absence of Mg^{2+}, employing different ligand: protein ratios, from 10:1 to 147:1. It can be observed that the increase in the free kanamycin-A fraction produces on the NMR spectra exactly the same effect previously observed in presence of the ion, which confirms that the observed decrease in the $\sigma_{H1-I/H4-II}/\sigma_{H1-I/H2-I}$ ratio mainly reflects the increase of the free ligand contribution to the average cross relaxation rates, and not a direct effect of Mg^{2+} on the antibiotic protein-bound conformation. This observation illustrates the importance of testing several ligand−protein ratios for analyzing of the protein-bound geometries of small ligands by trNOE measurements, especially for those systems characterized by k_{-1} values in the 10^2 s^{-1} range. Thus, given the large effect of Mg^{2+} on aminoglycoside binding, the free concentration of this ion was kept to a minimum in the analysis of the ternary complexes.

Comparison between the Experimental Data Measured with the Wild-Type ANT(4′) and Mutants 2–3. It should be mentioned that, at any Mg^{2+} concentration tested, the trNOE spectra obtained for the wild-type enzyme slightly differ from those measured for mutant-1 (for which the secondary aminoglycoside binding region B has been removed). These differences reflect the additional contribution to the observed cross-peaks of ligand binding to site B in the complex with the wild-type enzyme (Figure 6a). In fact, even, at 10 mM Mg^{2+}, clear trNOEs were detected for kanamycin-A in the presence of mutant-2, proving that binding to protein region B in wild-type ANT(4′) cannot be neglected (Figure 6b). Therefore, care should be taken when analyzing molecular recognition processes involving highly charged complexes for which multiple binding of the ligand to different protein regions must be carefully considered. Our data show that these secondary binding events can contribute to the measured trNOEs, even at large Mg^{2+} concentrations and basic pH values.

NMR Analysis of Kanamycin-A/ANT(4′) Ternary Complex. First, the ternary complex was analyzed employing the protein variant-1 and $CaCl_2$ instead of $MgCl_2$ to prevent catalysis. Typical spectra obtained for kanamycin-A (**1**) in the presence of ATP/Ca^{2+} at different ligand/protein regions are shown in Figure 7. Clear differences with respect to the data obtained for the binary complex or the free antibiotic (see Figure 5a,b) are evident. Thus, the H1−I/H3−II and H1−I/H5−II contacts, representative of an anti-Ψ orientation for the I/II linkage, are more intense than that observed for the H1–1/H2−I pair (corresponding to a fixed distance of 2.4 Å and used as reference). In addition, the relative intensity of the H1−I/H4−II NOE, characteristic of the syn-Ψ minimum, is clearly reduced. These data are consistent with a conformational selection of an anti-Ψ geometry for the I/II region of **1** (which would be in qualitative agreement with the X-ray data). In contrast, the III/II fragment exhibits a similar orientation to that measured in the binary complex or for the free antibiotic (characterized by a strong H1−III/H6−II cross-peak).

To evaluate the influence of spin diffusion on the measured trNOEs and to derive the precise geometrical features of **1** in the bound state, CORCEMA simulations were performed employing the crystallographic coordinates of the complex (considering those enzyme protons closer than 6 Å to the antibiotic, see the Materials and Methods section) and assuming different conformations for the antibiotic.

First, the kinetic parameters for the free/bound exchange process were estimated by fitting the NOE build-up curves to the intraresidue H1/H2 NOEs (corresponding to a fixed distance of 2.40 Å) in units I and III. In general a reasonable agreement between experimental and theoretical data was obtained employing τ_c(free) = 0.2 ns, τ_c(bound) = 60–70 ns, $K_a = 10^5$ M^{-1}, k_{-1} = 50–75 s^{-1} (see Figure S12). In a second step, these parameters were employed to simulate the NOE build-up curves for the structurally relevant cross-peaks assuming different conformations for the antibiotic (Figure 8). More specifically, the X-ray conformations of **1** in complex with ANT(4′) together with the minimum energy geometries syn-Ψ and anti-Ψ for each glycosidic linkage were considered.

In addition, different geometries, close to these minima were also considered until an optimal agreement between the theoretical and experimental trNOEs was obtained. These analyses allow discarding the X-ray geometries as the protein-bound conformation of kanamycin-A in solution and show that the experimental data can be reasonably fitted (Figure 8) by a single structure of the drug characterized by I/II and III/II glycosidic linkages in the anti-Ψ (Φ/Ψ –30°/−167°) and syn-Ψ (Φ/Ψ –4°/−11°) regions, respectively.

The X-ray structures of the complexed antibiotic,[21] with H1−I/H3−III distances much shorter than the H1−I/H5−III, fails to reproduce the NOE build-up curves for these key interresidue contacts (see Figure 8). In fact, a rotation of the Ψ angle corresponding to the I/II fragment of 41°/51° would be

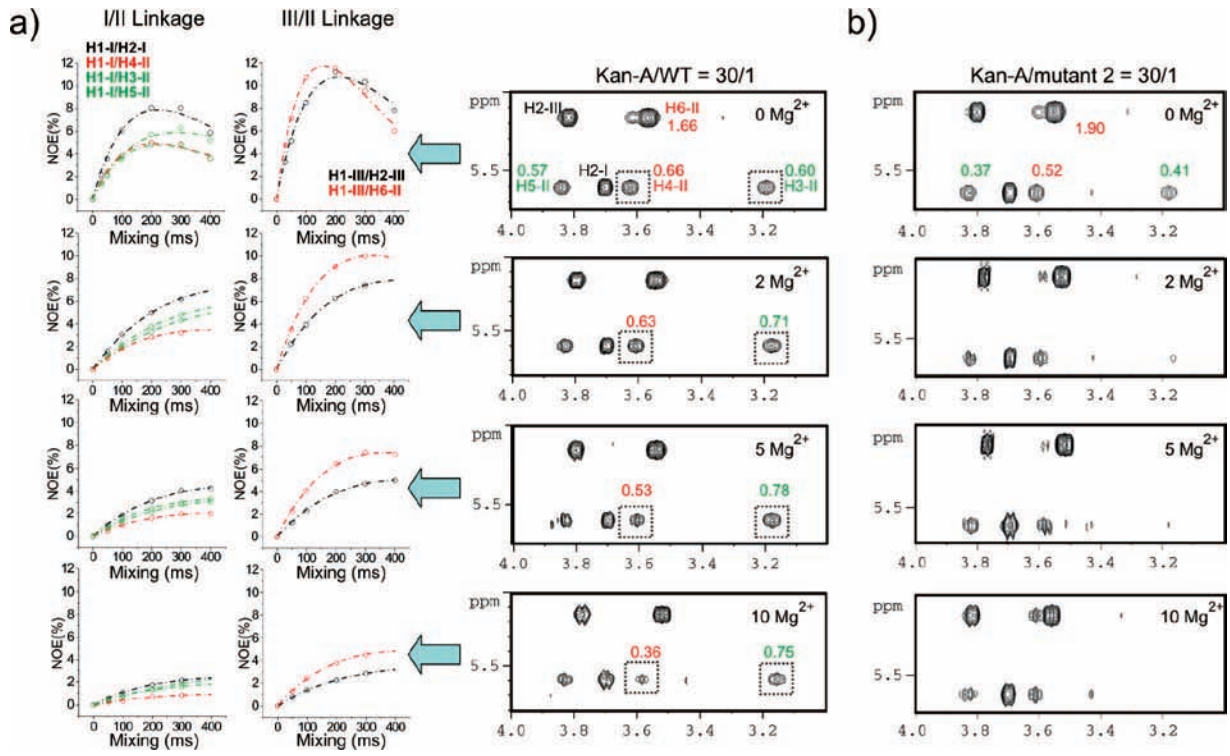

Figure 6. (a) trNOESY (mixing 100 ms) spectra acquired for kanamycin-A in the presence of the wild-type ANT(4′) at different Mg^{2+} concentration. Structurally relevant NOE build-up curves, for the I/II and III/II linkages are shown on the left. At 0 mM Mg^{2+}, the experimental ratios between the structurally relevant cross relaxation rates and those corresponding to the known fixed distances, H1−I/H2−I and H1−III/H2−III, for units I and III, respectively, are indicated. The effect of Mg^{2+} on the $\sigma_{H1-I/H4-II}/\sigma_{H1-I/H2-I}$ and $\sigma_{H1-I/H3-II}/\sigma_{H1-I/H2-I}$ ratios is highlighted. (b) trNOESY (mixing 100 ms) spectra acquired for kanamycin-A in the presence of mutant-2 at different Mg^{2+} concentration. Cross relaxation rates ratios at 0 mM Mg^{2+} are also indicated. These data strongly suggest that the binding of the antibiotic to protein site B has a certain contribution to the average cross-peaks observed in presence of the wild-type protein even at high pH values and Mg^{2+} concentrations.

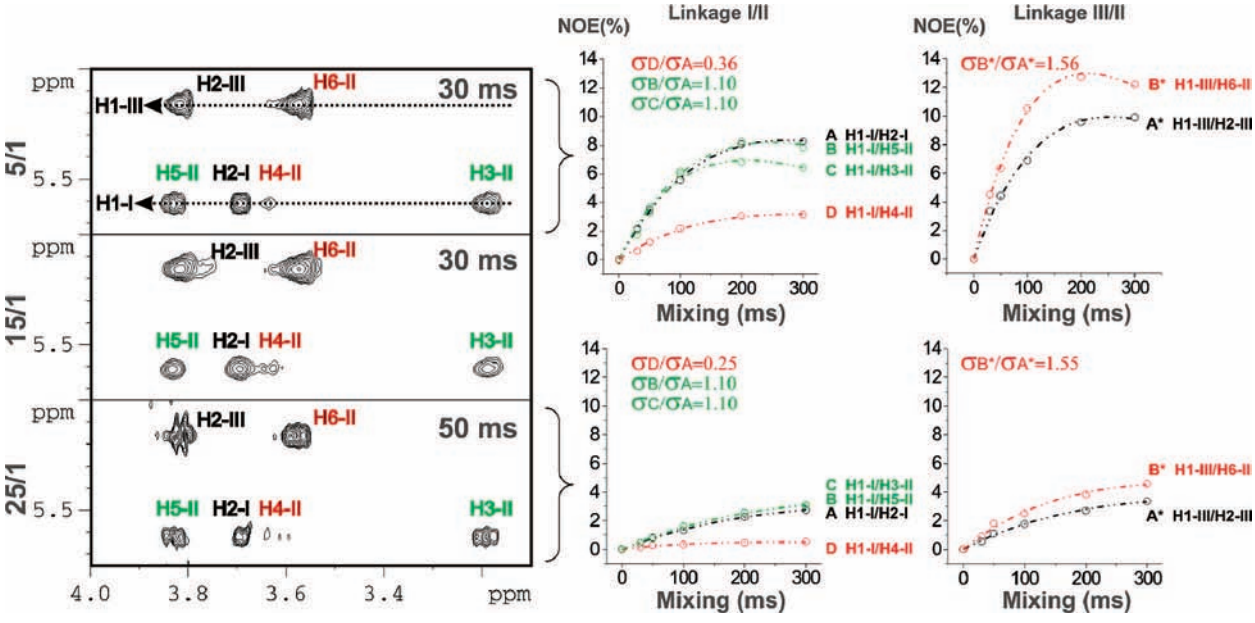

Figure 7. (Left) Key region of trNOESY spectra measured for the mutant-1/kanamycin-A/ATP ternary complex at different ligand/protein ratios from 5/1 to 25/1 (indicated on the left). The mixing time employed is indicated on the top-right corner for each case. NOEs representative of syn-Ψ and anti-Ψ minima are coloured in red and green, respectively. Structurally relevant NOE build-up curves measured at the two extreme ligand/protein ratios (5/1 and 25/1) are shown on the right. In addition, the ratios between the structurally relevant cross relaxation rates and those corresponding to the known fixed distances, H1−I/H2−I and H1−III/H2−III, for units I and III, respectively, are indicated.

required to get a reasonable agreement between theoretical and experimental data (Figure 9a).

It could be argued that NMR experiments were performed in the presence of ATP/Ca^{2+} while the crystallographic studies employed AMPCPP/Mg^{2+}. Therefore, the influence of AMPCPP/Mg^{2+} on the kanamycin-A protein-bound conformation was also analyzed. Figure 9b shows trNOESY spectra obtained for the aminoglycoside in the presence of mutant-1 and different

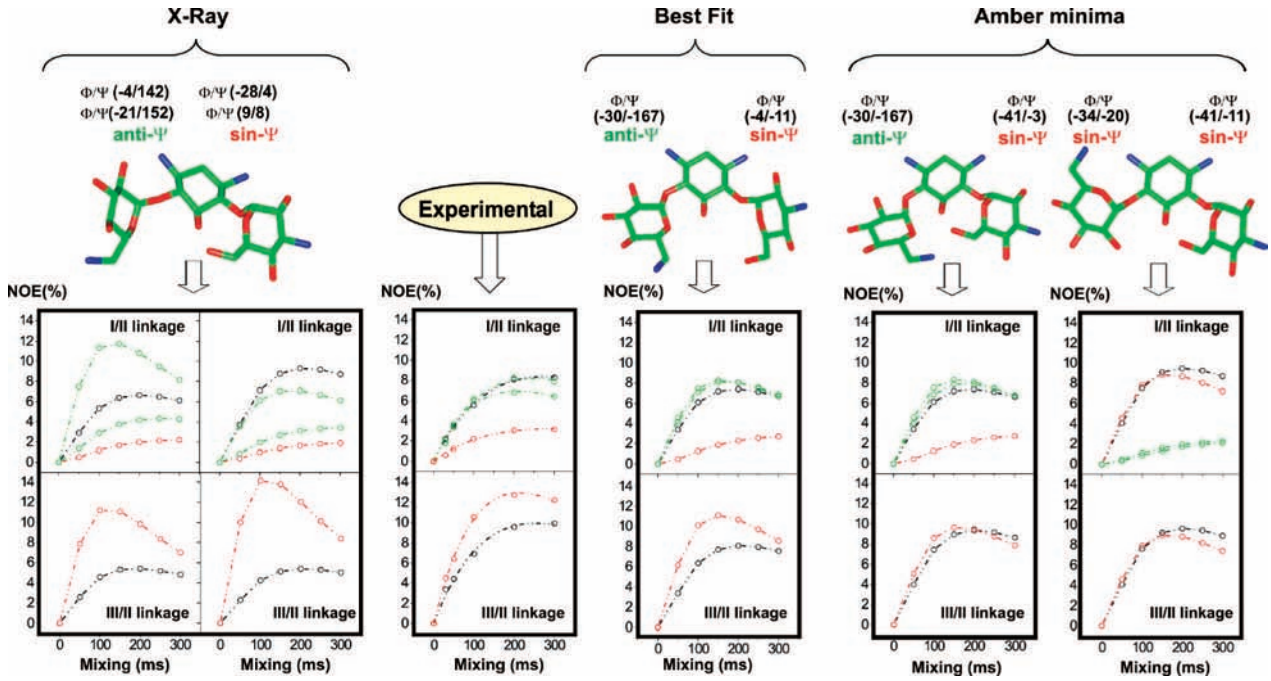

Figure 8. Experimental NOE build-up curves (middle panel) obtained for the mutant-1/kanamycin-A/ATP ternary complex (10 mM phosphate, pH 7.8, at 303 K), at 5/1 ligand/protein ratio, together with the theoretical curves (left and right panels) calculated with CORCEMA assuming different geometries for the drug-bound state; the X-ray structures (left, the two antibiotic molecules present per protein dimer exhibit slightly different geometries; both were employed in the calculations) and the two AMBER* minima (right). The antibiotic geometry that produces the best agreement with the experimental data is also shown. In all cases, NOE build-up curves representative of syn-Ψ and anti-Ψ low-energy regions are shown in red and green, respectively. Simulation parameters were [mutant-1] = 100 μM, [kanamycin-A] = 500 μM, τ_c(free) = 0.2 ns, τ_c(bound) = 60 ns, $K_b = 10^5$ M^{-1}, $k_{-1} = 75$ s^{-1}.

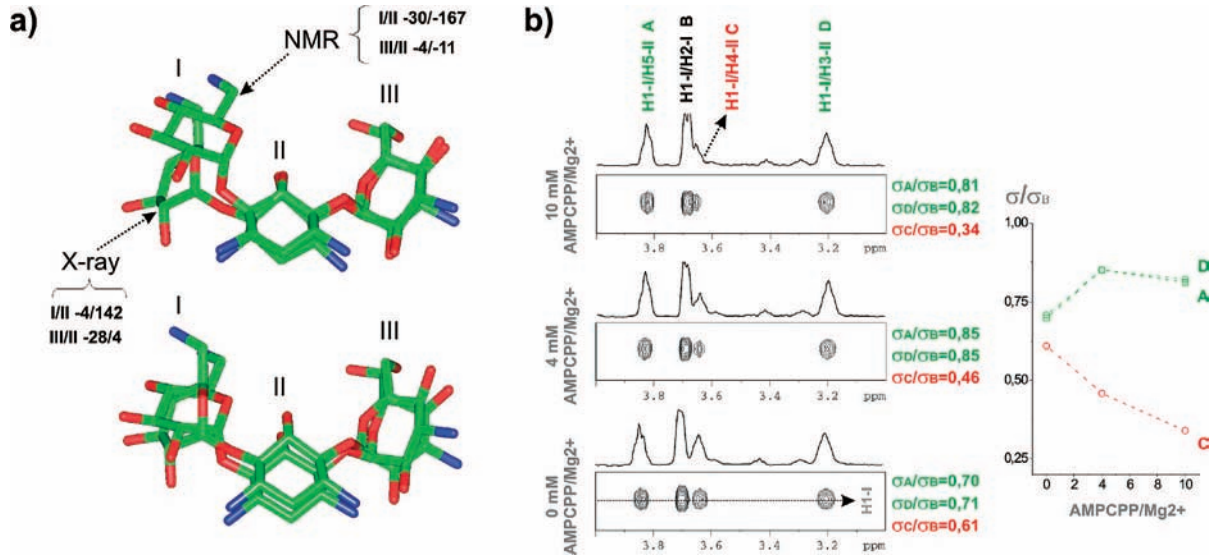

Figure 9. (a) Comparison between the conformation of kanamycin-A (**1**) bound to the protein site A, according to both NMR and the X-ray data. Superimpositions of heavy atoms in units II and III (top) and the three units (bottom) are shown. (b) Key region of trNOESY spectra (mixing 50 ms) measured for the kanamycin-A/AMPCPP/mutant-1 ternary complex at 10:1 antibiotic/protein ratio (1 mM kanamycin-A and 100 μM mutant-1) and several concentrations of AMPCPP/Mg^{2+}. NOEs from H1−I are shown. Cross-peaks representative of syn-Ψ and anti-Ψ minima are labelled in red and green, respectively. In addition, the ratios between the structurally relevant cross relaxation rates and those corresponding to the known fixed distance, H1−I/H2−I are also indicated. Variations in these ratios with the AMPCPP/Mg^{2+} concentration are graphically represented on the right.

concentrations of the nucleotide analogue. It can be observed that, also under these conditions, a clear decrease in the H1−I/H4−II cross relaxation rate is apparent, while the H1−I/H3−II and H1−I/H5−II trNOEs remain intense in all cases (the observed variation in the structurally relevant ratios $\sigma_{H1-I/H4-II}/\sigma_{H1-I/H2-I}$, $\sigma_{H1-I/H5-II}/\sigma_{H1-I/H2-I}$ and $\sigma_{H1-I/H3-II}/\sigma_{H1-I/H2-I}$ with the AMPCPP/Mg^{2+} concentration is also shown in Figure 9b). This fact is also consistent with a conformational selection of the anti-Ψ orientation for the I/II antibiotic region by the protein, and indicates that the substitution of ATP/Ca^{2+} by AMPCPP/Mg^{2+} has no effect on the aminoglycoside conformational features. However, larger concentrations of AMPCPP/Mg^{2+} were required to obtain a similar effect to that observed with ATP/Ca^{2+} suggesting a lower affinity of the protein for

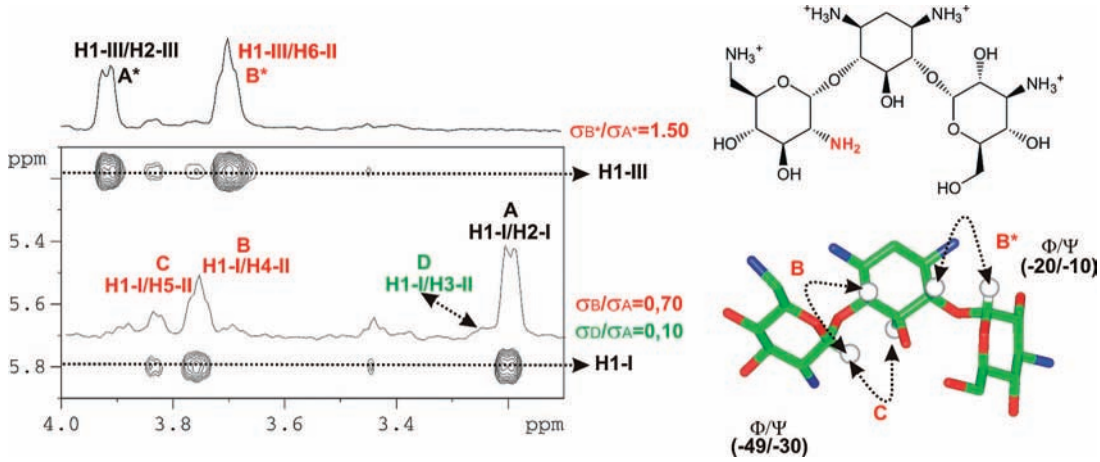

Figure 10. trNOESY spectrum (mixing 50 ms) measured for the kanamycin-B/AMPCPP/mutant-1 ternary complex. Traces in F1 at H1−I and H1−III frequencies are shown. The ratios between the structurally relevant cross relaxation rates and those corresponding to the known fixed distances, H1−I/H2−I and H1−III/H2−III, for units I and III, respectively, are indicated. Kanamycin-B protein-bound geometry is shown on the right together with the key contacts. The NMR data are consistent with a syn-Ψ arrangement for both glycosidic linkages.

the former molecule (in fact, protein crystals for the X-ray analysis were soaked in buffer with 16 mM AMPCPP for complex formation).[21]

General Conclusions from the Structural Analysis of Kanamycin-A Bound to the Catalytic Region of ANT(4′). Previous studies have shown that despite the apparent symmetry of kanamycin-A, the two glycosidic linkages present strikingly different conformational properties.[35] Thus, the III/II region is rigid under any pH conditions. In contrast, the conformational behavior of the I/II glycosidic linkage is extremely sensitive to the pH conditions and exhibits a large conformational heterogeneity at pH < 5.0 (the fully protonated form of the drug) that gradually decreases at neutral and basic pH values.

According to the trNOE spectra, in the absence of ATP, the binding of kanamycin-A (**1**) to the catalytic region of ANT(4′) (herein referred as region A) at pH 7.80 causes a significant increase in the internal mobility of the glycoside I/II linkage. In fact, the experimental data collected for the binary complex at basic pH resemble that measured for the free antibiotic at pH 4.0. The observed behavior could be explained by simply assuming that the antibiotic is fully protonated when bound to ANT(4′). This would not be surprising, as the linkage between binding and protonation has been proved in the past for the association of aminoglycosides to different protein and RNA receptors.[31–33]

In presence of both ATP/Ca^{2+} or AMPCPP/Mg^{2+} the protein selects a single conformation of the drug, characterized by the anti-Ψ orientation of the I//II linkage. Therefore, the binding process implies a conformational selection phenomenon. However, it should be taken in account that the energy cost of this selection is probably low, given the intrinsic flexibility of kanamycin-A (especially when is fully protonated).[35] The differences between the X-ray and NMR structure of the bound antibiotic (Figure 9a) could be simply attributed to the relatively low resolution of the crystallographic data (2.5 Å).

The Pattern of OH/NH_3^+ Substitution Is the Key Factor Determining the Aminoglycoside Protein-Bound Geometry: Comparison between Kanamycin-A and B Ternary Complexes. As a next step, the conformational properties of kanamycin-B (**2**) bound to the catalytic region of ANT(4′) (herein referred as site A) were subjected to a NMR analysis. This antibiotic shares an identical covalent scaffold with kanamycin-A (**1**), differing in just a single position (an OH/NH_3^+ substitution at position 2 of ring I, see Figure 10). However, previous studies have shown that this slight difference produces a significant alteration on the antibiotic conformational properties. For kanamycin-B both I/II and III/II glycosidic bonds are extremely rigid and exhibit a dominant syn-Ψ orientation under any pH conditions.[35] This implies that any conformational deviation from the syn-Ψ low-energy region (as that observed for **1** complexed to ANT(4′)) would represent a significant cost in energy. Therefore, the assumption of a similar protein-bound conformation for both antibiotics is not justified.

First attempts to form the ternary complex were performed employing mutant-1 and ATP/Ca^{2+}. Surprisingly, in this case, at the large protein concentration employed in the NMR experiments (100 μM), the nucleotidylation reaction proceeded slowly to completion, showing that the ATP/Ca^{2+} complex behaves as a bad substrate when the antibiotic is kanamycin-B (and not as a competitive inhibitor, as in the kanamycin-A case). Therefore, further studies were performed using AMPCPP/Mg^{2+}.

TrNOESY spectra were acquired at different concentrations of AMPPCPP/Mg^{2+} from 2 to 10 mM (see Figure 10). In all cases, the NMR data were consistent with a single syn-Ψ orientation for both glycosidic linkages (characterized by strong H1−I/H4−II and H1−III/H6−II cross-peaks), in contrast with the behavior exhibited by **1**. Thus, the kanamycin-B protein-bound structure is similar to that detected for this antibiotic in the absence of the protein.

The structure of different aminoglycosides closely related to kanamycin, in complex with their target A-site RNA, has been described in recent years by X-ray methods. All these ligands share the same covalent scaffold, differing mainly in the pattern of OH/NH_2/NH_3^+ substitution at various positions. Previous studies have shown that these subtle differences may have a large influence on their conformational preferences.[35] Interestingly, according to the X-ray data, all of them bind to the RNA receptor in exactly the same manner. For example, for the closely related antibiotics kanamycin-A (**1**), tobramycin (**3**), amikacine (**4**), and gentamycin (**5**), the pairwise rmsd for heavy atom superimposition in the RNA-bound state is only 0.31 Å. (see Figure 11).[7a–c]

Inspection of the crystallographic data reveals that all the complexes are stabilized by a similar combination of electro-

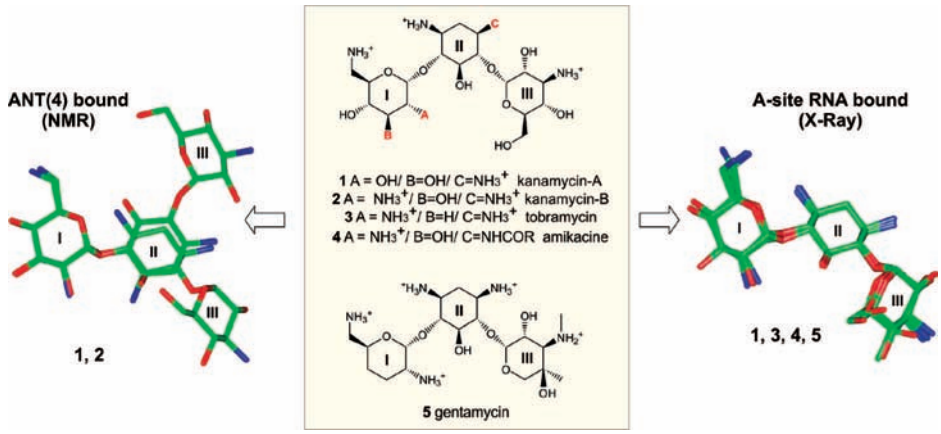

Figure 11. Middle panel: Schematic representation of several antibiotics (**1**−**5**) of the 4,6 2-DOS subfamily. All these compounds share an identical covalent scaffold differing in the pattern of $OH/NH_2/NH_3^+$ substitution. Right panel: Structure of aminoglycosides **1**, **3**−**5** bound to their target A-site RNA according to X-ray studies. For amikacin (**4**) the substituent NHCOR at position 1−II is not shown for simplicity. Despite the differences in charge distribution, all of them adopt an identical conformation within the RNA binding pocket. Left panel: Structure of kanamycin-A (**1**) and B (**2**) bound to ANT(4′) (ternary complexes). Although these compounds differ only in a single position, they are recognized by the enzyme in different conformations.

static, polar, and stacking interactions. Some of these contacts are shape sensitive, which explains why antibiotics with the same covalent scaffold share also similar binding modes. The binding of kanamycin to the nucleotidyltrasnsferase ANT(4′) represents a totally different process. In this case, the protein/aminoglycoside complex is exclusively stabilized by electrostatic and polar contacts between glutamate/aspartate side chains and the antibiotic $OH/NH_2/NH_3^+$ groups. These interactions are less sensitive to the global shape of the drug. In fact, we have shown that although kanamycin-A (**1**) and B (**2**) differ only in a single position they are recognized by the enzyme in different conformations which indicates that the protein binding region A can accommodate different geometries of the aminoglycoside and therefore this factor is not critical for its inactivation. It would be tempting to describe complex formation as a *non-specific* process (characterized by the superimposition of multiple binding modes of comparable stabilities). However, there is some evidence against this consideration. First, a clear electron density is observed for the aminoglycoside in the X-ray ANT(4′)/kanamycin-A/AMPCPP crystallographic complex. In contrast, no electron density is detected at site B suggesting a highly dynamic nonspecific binding mode at this protein region.[21] Second, molecular recognition of **1** by ANT(4′) implies the selection of a unique conformational state, which is minor for the free antibiotic, under identical conditions. Third, despite the apparent symmetry exhibited by all aminoglycosides, within this subfamily, the adenylation reaction proceeds with significant regioselectivity. In fact, previous studies have failed to identified any additional product apart from that resulting from kanamycin-A modification at position 4 of ring I.[24] Finally, close inspection of the ANT(4′)-bound conformations of **1** and **2** shows that, despite the obvious differences in global shape, they might exhibit a similar spatial distribution for those key positive charges around rings I and II, involved in direct contacts with the protein. Figure 12a shows schematically the antibiotic/protein interactions established in the complexed state by kanamacyn-A (**1**), according to the X-ray data, together with a model of the kanamycin-B/ANT(4′) interaction, based on the NMR and X-ray data. For **1**, positions 2−I and 3−II participate in bifurcated hydrogen bonds with the side chain of E141. This contact is likely to be responsible for the stabilization of the unusual anti-Ψ orientation exhibited by the I/II linkage within the protein binding site A. For kanamycin-B (**2**) the energetically expensive[35] syn-Ψ/anti-Ψ conformational change would not be required, since an equivalent contact is possible for a syn-Ψ orientation of the I/II bond. In this case, the aminoglycoside would interact with E141 through positions 2−I and 5−II. Thus, although the protein-bound geometries of kanamycin-A and -B are different, the enzyme might recognize a similar spatial distribution of positive charges in both cases. Thus, charge distribution (and not strictly the global shape) seems to be the critical factor for aminoglycoside recognition and inactivation by ANT(4′) and could be at the origin of the regioselectivity exhibited by the enzyme.

Finally, the different conformation adopted by the I/II linkage in both kanamycin-A and B leads to a totally different orientation of ring III within the protein binding region. Thus for kanamycin-A, units III of two different antibiotic molecules are involved in direct hydrogen-bonding interactions (as previously mentioned, the binding sites for the two kanamycin molecules within the protein dimer are located at contiguous positions, see Figure 1). For kanamycin-B, this contact is not possible. Unfortunately, the accurate modeling of the ANT(4′)/kanamycin-B/AMPCPP complex would require a previous knowledge of the ionization state of all the glutamate/aspartate side chains present in the protein binding site, and the pK_a values for these residues in the complexed state are not available at present moment. However, the inspection of preliminary models, built assuming full ionization of the protein region A, permitted the suggestion that unit III of kanamycin-B can be easily accommodated at site A, without destabilizing steric contacts with the protein, and might even participate in polar interactions with the side chain of E93, thus contributing to complex stability (see Supporting Information Figure S13).

Effect of the Aminoglycoside Charge Distribution on the Enzyme Selectivity: Testing ANT(4′) against KanB/KanA and KanB/KanB Hybrids. Previous studies have failed to identify any product from adenylation reaction mixtures, excluding the kanamycin derivative modified at position 4 of ring I.[24] Given the polar/electrostatic nature of the antibiotic/ANT(4′) interaction and the symmetry that exists within the kanamycin molecule, this result might seem surprising. Indeed, considering the protein-bound conformation of kanamycin-A/B, an alternative binding mode could be proposed, in which rings I and III exchange their positions within the enzyme catalytic site. As shown in Figure 13, for compound **1**, both binding modes

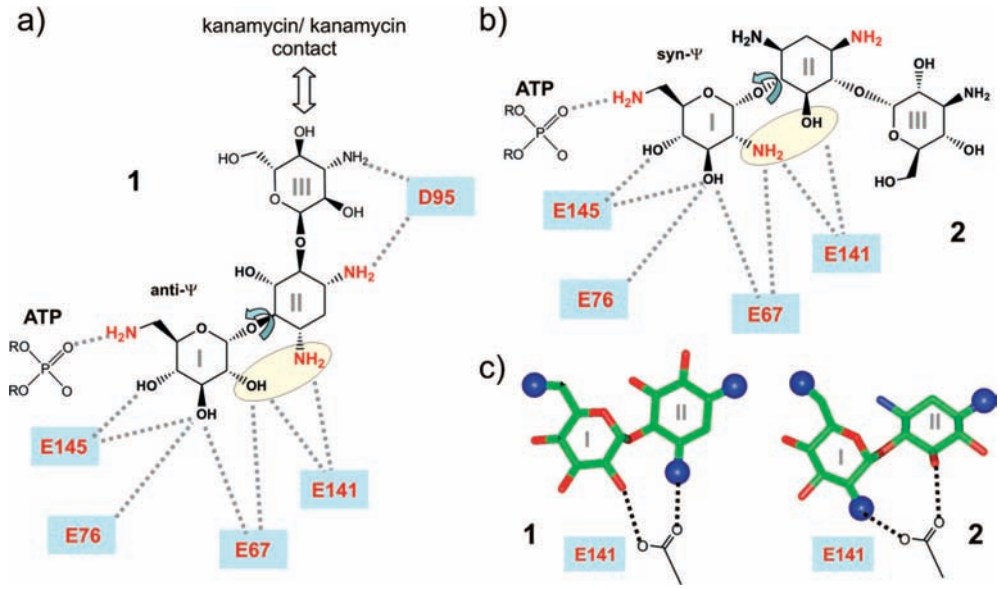

Figure 12. (a) Schematic representation of kanamycin-A (**1**) bound to ANT(4′). Protein/ligand interactions observed in the X-ray structure are indicated. Most contacts involved the aminoglycoside rings I/II. Positions 2−I and 3−II (highlighted in yellow) are involved in a bifurcated hydrogen bond with the side chain of E141. This contact would be responsible for the stabilization of the unusual anti-Ψ orientation exhibited by the I/II linkage in the complexed state. (b) Equivalent interactions at the key I/II region can be proposed for kanamycin-B (**2**) assuming a syn-Ψ arrangement. This conformation leads to a totally different location for unit III. (c) Bioactive conformation of the I/II fragment in kanamycin-A (**1**) and B (**2**). The antibiotic interaction with E141 side chain is schematically represented. Kanamycin-A amino groups involved in contacts with the protein together with those at equivalent positions in **2** are represented as spheres.

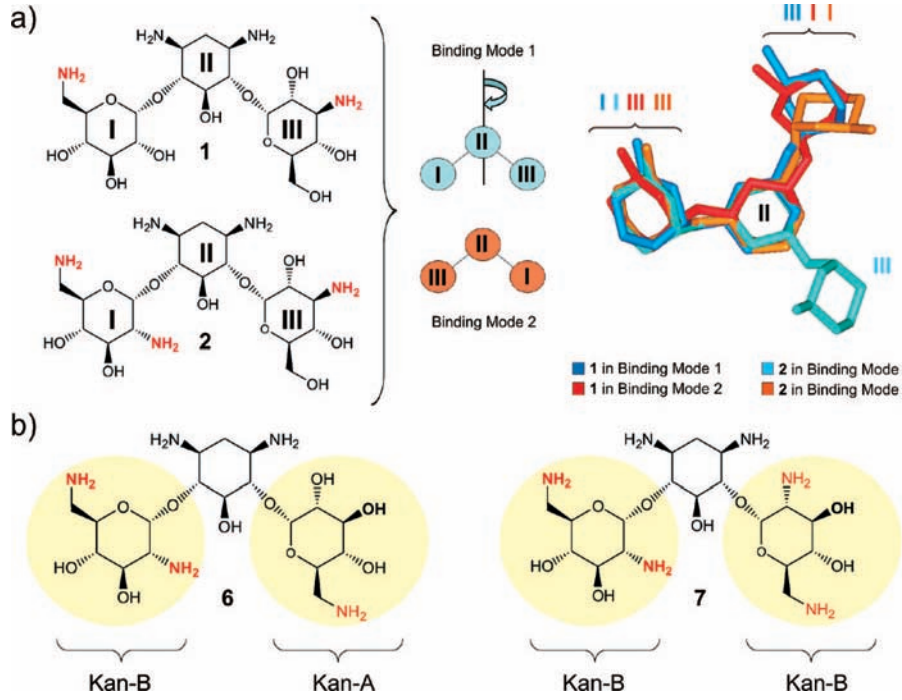

Figure 13. (a) Schematic representation of kanamycin-A (**1**) and B (**2**). Considering the protein-bound conformation of both antibiotics, an alternative binding mode (herein referred as 2) could be proposed in which rings I and III exchange their positions within the enzyme catalytic site. A heavy atom superimposition of the two proposed modes of interaction for aminoglycosides **1** and **2** is shown on the right. For simplicity, the OH and NH_2/NH_3^+ substituents are not shown. It can be observed that for compound **1**, both binding modes (in blue and red) are almost equivalent if we attend to the global shape of the drug. For **2**, the alternative binding mode (represented in orange) exhibits a global shape similar to that observed for **1** in the protein-bound state. (b) Schematic representation of the synthesized kan-B/kan-A (**6**) and kan-B/kan-B (**7**) hybrids.

(related by a 180° rotation around the streptamine unit, ring II, and represented in blue and red in Figure 13) are almost equivalent if we consider the global shape of the ligand. In addition, for **2** the alternative binding mode (represented in orange in Figure 13) exhibits a global shape similar to that observed for **1** in the protein-bound state.

However, we have proposed above, that the global shape is not a critical factor for aminoglycoside binding and inactivation. Our results show that the $OH/NH_2/NH_3^+$ distribution within the aminoglycoside scaffold governs the preferred binding mode of the aminoglycoside. This feature might also be at the origin of the enzyme regioselectivity. To test this hypothesis, we

Table 2. Time Evolution of Reaction Mixtures Containing 2 mM Aminoglycoside (**1**, **2**, **6** and **7**), 8 mM ATP, 10 mM $MgCl_2$ in 10 mM Phosphate (pH 7.5) upon Addition of 7 μM Wild-Type ANT(4′)[a]

	kanamycin-A (1)				kanamycin-B (2)			derivative 6			derivative 7		
time	**1**	**1**-A	**1**-A_2	time	**2**	**2**-A	**2**-A_2	**6**	**6**-A	**6**-A_2	**7**	**7**-A	**7**-A_2
0	100	0	0	0	100	0	0	100	0	0	100	0	0
25	55	45	0	4	55	45	0	40	60	0	65	35	0
90	30	70	0	14	15	85	0	0	100	0	35	55	10
120 (+E)	8	84	8	24	0	96	4	0	90	10	20	50	30
360	0	50	50	34	0	94	6	0	80	20	15	40	45
600	0	25	75	44	0	92	8	0	70	30	5	30	65
840	0	10	90	54	0	89	11	0	60	40	0	20	80
1600	0	5	95	64	0	86	14	0	50	50	0	10	90

[a] The estimated populations (%) for the unmodified, mono (-A) and diadenylated (-A2) -aminoglycosides are shown. For kanamycin-A (1) fresh ANT(4′) was added after 120 min (from that point the total ANT(4′) concentration in the NMR tube was 27 μM). Time is given in minutes.

synthesized two hybrid kanamycin derivatives (KanB/KanA **6** and KanB/KanB **7**, see Figures 13, S14, and S15). In these compounds the pattern of $OH/NH_2/NH_3^+$ substitution at ring III was modified to match that present in unit I of both kanamycin-A (**1**) and B (**2**). Then, the regioselectivity of the adenylation reaction against these derivatives was analyzed. As a preliminary control, enzymatic reactions were performed employing kanamycin-A and -B. ATP/Mg^{2+} (8/10 mM) and the aminoglycosides (2 mM) were dissolved in phosphate buffer (10 mM pH 7.5). After addition of the enzyme (7 μM), the evolution of the reaction mixture at 308 K was monitored by 1D NMR, and the final products were characterized by 2D-NMR and MALDI-TOF MS. The obtained results are summarized in Table 1 (see also Figure S16). For **1**, the nucleotidylation proceeded smoothly until completion (in 2 h), to produce the expected monoadenlylated derivative. At this point, an extra amount of protein (+20 μM) was added to the NMR tube (indicated in Table 2 and Figure S16 by +E), and the evolution of the reaction mixture was monitored over longer periods. It can be observed that the diadenylated adduct, at positions 4−I and 4−III is indeed formed at a very slow rate but with high selectivity (the reaction is almost complete after 18 h at 35 °C; see also Figures S16 and S17).

For compounds **2**, **6**, and **7**, the whole reaction was performed at 7 μM protein concentration. The obtained results (shown in Table 2 and Figure S16) are in agreement with the previously mentioned hypothesis and conclusively show that the spatial distribution of $OH/NH_2/NH_3^+$ groups within the aminoglycoside scaffold is the key factor that determines the regioselectivity of the reaction (see Table 2 and Figures S16−S18). More specifically, the presence of NH_2/NH_3^+ functions at positions 2 and/or 6 of glucose ring III (or I) strongly promotes its enzymatic modification by ANT(4′). Thus, for those compounds that include 6 amino-glucose (**6**) or 2,6 diamino glucose (**7**) as ring III the diadenylation reaction is significantly faster. Interestingly, in compound **7** the enzyme still shows a certain preference for ring I. This might be attributed to differences in the pK_a values of the amino functions located at this unit with respect to those present in unit III.

As a final step we analyzed how sensitive the inactivation process is to the net positive charge around the antibiotic units I and III. Given the large density of acid residues (E145, E76, E67, E141, and the nucleotide triphosphate moiety) around kanamycin-A unit I, in the crystallographic complex it could be hypothesized that the net positive charge exhibited by this ligand region is important for binding and inactivation.

In fact, this feature should be dominant for a purely nonspecific binding process. Moreover, due to the internal symmetry that exists within this family of antibiotics, the balance of positive charges between rings I and III should be carefully considered. Thus, it might be speculated that by altering this balance it should be possible to promote alternative binding modes (equivalent to those previously proposed), in which ring III occupies the location where unit I is placed within the kanamycinA/ANT(4′) X-ray complex. If these modes of interaction are productive this would lead to a change in the enzyme selectivity. Otherwise they would be expected to compete with the productive binding mode decreasing the apparent enzyme activity for a given substrate. To analyze this question, derivatives **8**−**10** were synthesized, and the activities of wild-type ANT(4′) against them were compared to those measured for the natural compounds **1** and **2**. All these aminoglycosides exhibit differences in the number of positive charges around rings I/III varying from +2/0, as in derivative **8**, to +1/+3, as in derivative **10** (see Figures 14, S19 and S20).

First, adenylation reactions were performed in NMR tubes and monitored by 1D-NMR. As expected from the results reported above, compounds **1**, **2**, and **8**−**10** (Figure 14) were selectively modified on ring I which confirms that the particular location of the NH_2/NH_3^+ groups within the aminoglycoside scaffold, and not the balance of positive charges between units I/III, is the key factor that determines the regioselectivity of the reaction (in all cases adenylation at unit III was either not detected or extremely slow).

As a second step, the apparent kinetic parameters for the adenylation reaction were derived (see the Materials and Methods section). The presence of nonproductive binding modes should affect the kinetic parameters of the reaction, leading to a decrease in the apparent k_{cat} and K_M values.[36] The obtained results (represented in Figure 14) provide no evidence in favor of alternative nonproductive binding modes for those derivatives more heavily charged at ring III (in fact they tend to exhibit larger values for both k_{cat} and K_m) suggesting that the balance of positive charges in rings I/III does not determine the aminoglycoside binding mode to ANT(4′) catalytic site A. Instead, this process is probably sensitive to the particular location of the amino groups within the antibiotic scaffold. This could seem unreasonable given the electrostatic nature of the aminoglycoside/enzyme interaction. However, it should be taken into account that aspartate/glutamate side chains involved in antibiotic recognition at site A might exhibit significantly altered pK_a values. Indeed it is feasible that even at pH > 7.0 some of them remain protonated. In our opinion, the spatial distribution of negative charges generated by these strongly coupled acid residues might match the distribution of positive charges in the natural drug being, at least in part, responsible for the formation of a preferred productive complex.

Interestingly, kanamycin-A derivatives with more amino functions placed on ring III exhibit significantly larger values of K_m. The origin of this effect is unknown. However, a possible explanation could be found by examining the structural data available. Thus, according to the X-ray data, unit III of two different kanamycin-A molecules present direct interactions within the kanamycin-A/ATP/ANT(4′) ternary complex. There-

(36) Fersht, A. In *Enzyme Structure and Mechanism*; W. H. Freeman and Co.: New York, 1985; 342–343.

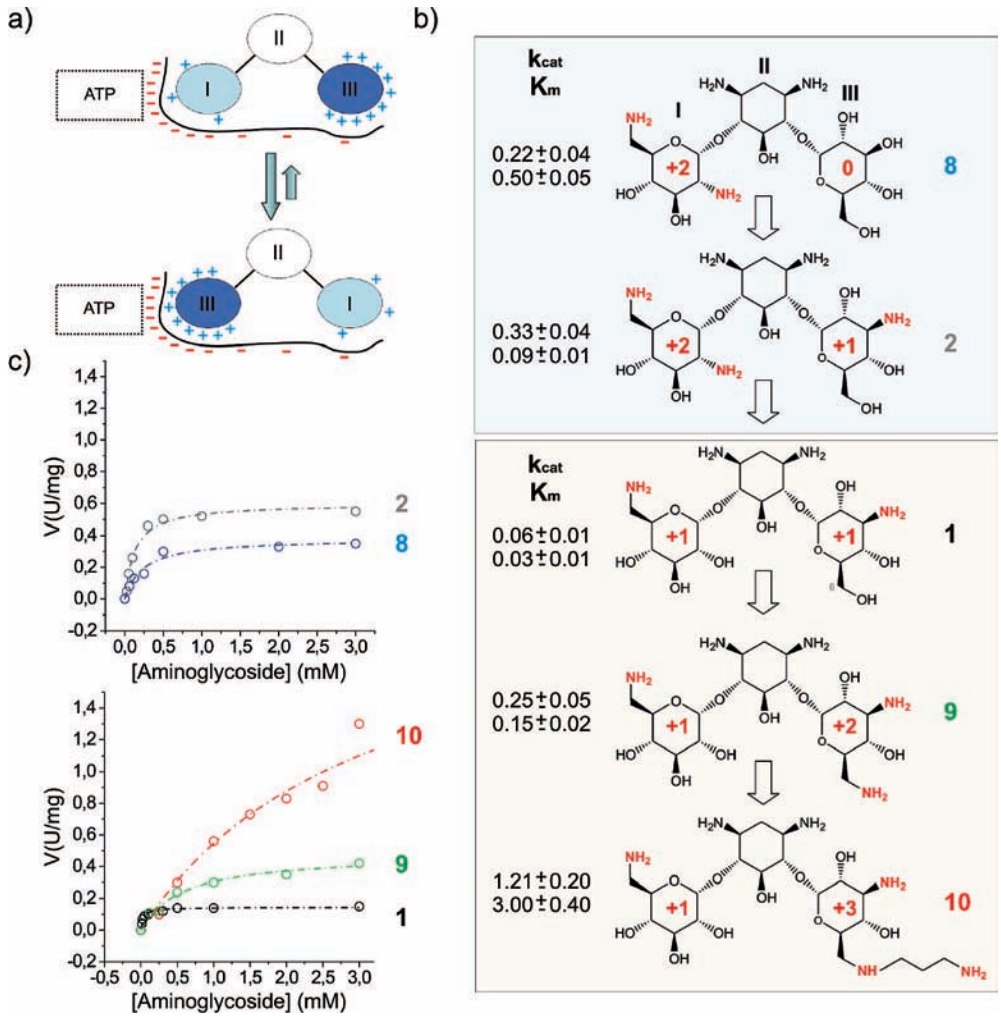

Figure 14. (a) Schematic representation of the proposed alternative binding modes. (b) Enzymatic activity of wild-type ANT(4′) against several natural (**1** and **2**) and newly synthesised (**8**, **9**, and **10**) kanamycin derivatives. These compounds present a different number of positive charges around rings I and III (varying from +2/0, as in derivative **8** to +1/+3, in derivative **10**). (c) Protein activity at increasing concentrations of aminoglycosides **1** and **2** and **8**−**10**. Data were fitted to hyperbolic curves. K_m and k_{cat} values are given in mM and s^{-1} units, respectively. The reported values are an average of three independent experiments.

fore, the repulsion between positive charges at these rings could be at the origin of the observed increase in the apparent K_m for derivatives **9** and **10**.

Conclusions

We have shown that the possibility of multiple binding should be taken into account in the NMR analysis of complex molecular recognition processes involving highly charged species. The ANT(4′)/aminoglycoside system represents a key example of this situation. Our results indicate that, in favorable cases, the different binding events can be separated and analyzed independently employing site-directed mutagenesis. Thus, for ANT(4′) two different aminoglycoside binding sites, referred as A and B throughout the manuscript, have been identified and isolated in multiple mutants of the enzyme.

Site B represents a nonspecific aminoglycoside binding site. This consideration is supported by the fact that no electron density is observed at this protein region within the ANT(4′)/kanamycin-A (**1**)/AMPCPP complex described by X-ray methods. Our analysis reveals that aminoglycoside binding to this secondary site contributes to the observed trNOEs in the wild-type enzyme, even at high Mg^{2+} concentration and basic pH values (pH 7.8). This superimposition of different binding events, in the wild-type protein, represents a serious problem in the analysis of the NMR data.

Site A is located at the catalytic center of ANT(4′) and was first characterized by X-ray methods. In the absence of the nucleotide, the NMR data indicates a significant increase in the antibiotic mobility upon binding to this protein region, which is consistent with an alteration in the kanamycin-A (**1**) protonation state. In fact, aminoglycoside binding to both RNA and proteins has been shown to be linked to the protonation of the antibiotic, in different systems. In contrast, formation of the ternary complex implies a conformational selection phenomenon. Thus an anti-Ψ conformation, which is minor for the free antibiotic, under identical conditions, is recognized by the enzyme. The NMR-derived protein-bound structure of **1** is slightly different from that derived by crystallography, which can be attributed to the relatively low resolution of the X-ray data.

In addition, we have shown that the spatial charge distribution of the drug around rings I and II determines its geometrical features bound to the catalytic A region. In contrast, the global shape of the antibiotic does not seem to be a critical factor. This represents a qualitative difference between the molecular recognition of kanamycin by the target A-site RNA and the

resistance enzyme ANT(4′). Thus, although kanamycin-A (**1**) and B (**2**) share an identical covalent scaffold, differing in a single position (an OH/NH_3^+ substitution at position 2 of ring I, see Figure 1), they interact with the enzyme adopting rather different geometries. Close inspection of the bioactive conformation for both compounds strongly suggests that, despite the obvious differences in global shape, both structures present a similar spatial distribution of positive charges around rings I and II. Therefore, the enzyme seems to be able to discriminate between different charge distributions. This conclusion is further supported by measurements of the enzymatic activity and regioselectivity displayed by the wild-type protein with modified kanamycin derivatives and explains the preferred adenylation of ring I in natural kanamycin-A.

Finally, some comments regarding the implications of these results for drug design should be made. Previous studies, by our group, have shown that conformational restriction of the aminoglycosides can, in favorable cases, prevent the antibiotic inactivation by ANT(4′).[19] Thus, considering the ANT(4′)-bound conformation of kanamycin-A revealed by the X-ray data, we designed several neomycin-B derivatives with the I/II disaccharide fragment locked in the syn-Ψ conformation (Figure S21).These analogues were supposed to be protected against the enzymatic modification as they can not adopt the "bioactive" anti-Ψ orientation of the I/II linkage, observed in the crystallographic complex. Interestingly, only the most tightly constrained derivative (**11** in figure S21) behaved as a nonsubstrate, whereas those in which the restriction allowed wide fluctuations within the syn-Ψ low energy region were inactivated by the enzyme. The results reported herein provide a simple explanation for this observation. First, they show that the conformational features observed for kanamycin-A, in the protein-bound state, can not be extrapolated to other aminoglycosides, even within the same family. Thus, minor differences in the pattern of $OH/NH_2/NH_3^+$ substitution (kanamycin-A vs kanamycin-B) can lead to a different protein-bound geometry of the drug. In fact, according to our data, ANT(4′) exhibits a significant tolerance to conformational variations of the antibiotic. It is likely that minor fluctuations of the aminoglycoside I/II glycosidic linkage and/or small distortions in ring I puckering are required for catalysis, which might explain why tightly constrained neomycin-B derivatives (as **11**) are not susceptible to the enzymatic adenylation. However, both anti-Ψ and syn-Ψ orientations of the I/II linkage can be recognized and inactivated by ANT(4′), as proved by the trNOE measurements herein reported. This conclusion poses limitations on the conformational restriction as strategy in the design of new antibiotic derivatives *resistant* to ANT(4′).

On the other hand, we have also shown that the spatial distribution of NH_2/NH_3^+ groups around rings I/II (and not just the number of positive charges) determines the preferred binding mode of the drug and the regioselectivity of the reaction. More specifically, amino groups at positions 2 and 6 of ring I seem to be required for efficient aminoglycoside inactivation. It is well established that both functions also modulate the binding properties of the drug to the target A-site RNA.[7] However, they do not seem to be critical for RNA binding. In fact, there are examples of natural aminoglycosides lacking NH_2/NH_3^+ groups at either position 6 (as paromomycin) or 2 (as kanamycin-A) of ring I. Taking this into account, it seems feasible that alternative patterns of $OH/NH_2/NH_3^+$ substitution around units I/II might lead to new derivatives characterized by a significant antibiotic activity and a much reduced susceptibility to enzymatic inactivation by ANT(4′).

Materials and Methods

Kanamycin-A (**1**), and -B (**2**) were purchased from Sigma-Aldrich. Aminoglycoside derivatives **6** and **8** were prepared from neomycin following the procedure described by Chang et al.[37] The synthesis of kanamycin derivatives **7**, **9**−**10** will be described elsewhere.

Site-Directed Mutagenesis. The described mutations were incorporated into the wild-type gene of the *Staphylococcus aureus* ANT(4′) located on plasmid pET28b-*ant(4′)* using the QuitChange mutagenesis kit (Stratagene, La Jolla, CA). The appropriate mutagenic primers were used, in combination with 20 ng of template DNA, in Pfu DNA polymerase-catalyzed PCR reactions. Afterward, parental DNA was digested (1 h at 37 °C) with *DpnI* and the mutant plasmid DNA was transformed into $CaCl_2$ competent *Escherichia coli* BL21(DE3). Sequences of all constructs were confirmed by DNA sequencing.

Protein Expression and Purification. Selected clones for the ANT(4′) variants were grown on 100 mL of LB medium containing 26 μg /mL kanamycin at 37 °C. When the cell growth reached an optical density at 600 nm (OD_{600}) of 0.5, the temperature was switched to 30 °C and the culture was induced with 0.5 mM IPTG. After 24 h of induction, the cells were collected by centrifugation at 12000 rpm, resuspended in 50 mM Tris buffer, 1 mM EDTA, lysozyme (0.2 μg/mL), pH 8.2 and DNase I (1μg/mL) and stirred for 30 min. The cells were then lysed by passage though a French press and cell debris was removed by centrifugation at 13000 rpm for 30 min. Monosulphate streptomycin (1%) was added to the supernatant and this mixture was stirred for 30 min and then centrifuged at 12000 rpm. SDS-PAGE analysis of the obtained cell-free extract showed an overexpression band in all mutants. For the purification of the recombinant proteins containing an N-terminal 6-His tag, 12 mL of the cell-free extract were loaded into a Ni^{2+}-DA-agarose column (10 mL) pre-equilibrated with 40 mM imidazole (20 mM sodium phosphate, pH 7.5). After washing with the same buffer, the ANT(4′) variants were eluted with phosphate buffer containing imidazole 0.5 M. Fractions of 5 mL were collected and all fractions containing protein were pooled together and dialysed against water pH 7.8 and then lyophilized. After this step the enzymes were found to be more than 95% pure as assessed by SDS-polyacrylamide gel electrophoresis.

Analytical Ultracentrifugation Experiments—Sedimentation Equilibrium. The experiments were performed at 25 °C using a Beckman Optima XL-A analytical ultracentrifuge equipped with absorbance optics, using an An50Ti rotor. Whole-cell buoyant molecular masses ($M^c_{w,a}$) were determined by fitting a sedimentation equilibrium model for a single sediment solute to individual data sets with the program EQASSOC (supplied by Beckman).

CD Experiments. Circular dichroism spectra were recorded on a JASCO J-810 spectropolarimeter fitted with a peltier temperature control accessory. Far-UV spectra were recorded in 1 cm path length quartz cells at protein concentrations of 0.1 mg mL^{-1}. The CD spectrum of the buffer was subtracted from the experimental spectra. Final spectra were the average of 3 runs. Thermal denaturation experiments were carried out by increasing the temperature from 283 to 353 K at two different rates (20 and 40 deg h^{-1}) and monitoring changes in ellipticity at 222 nm. The obtained denaturation curves were analyzed by fitting the experimental data to a two-state model.

ITC Experiments. Isothermal titration experiments were performed at 298 K in 10 mM phosphate buffer (pH 7.0 and 7.8), unless otherwise stated, using a MCS-ITC microcalorimeter (Mi-

(37) (a) Wang, J.; Li, J.; Cheng, H.; Chang, H.; Tanifum, C. T.; Liu, H.; Czyryca, P. G.; Chang, C. T. *J. Med. Chem.* **2004**, *6*, 1381–1384. (b) Li, J.; Wang, J.; Czyryca, P. G.; Chang, H.; Orsak, T. W.; Evanson, R.; Chang, C. T. *Org. Lett.* **2004**, *6*, 1381–1384.

crocal, Inc.). Protein samples were extensively dialyzed against this buffer that was also used to dissolve kanamycin-A. Before the ITC measurements, the pH of the antibiotic stock solution was accurately adjusted to the value measured for the dialysis buffer, after allowing them to equilibrate at 25 °C in order to minimize errors. The titration curves were measured by stepwise injection of a concentrated solution of antibiotic (5–15 mM) into the reaction cell loaded with the protein solution (~1.35 mL). Typical protein concentrations in the calorimetric cell were in the 40–60 μM range (expressed as moles of dimer). For each/every experiment, the heat of dilution of kanamycin-A was measured in parallel (by injecting the antibiotic into the dialysis buffer) and the value was substracted from the heat of reaction. The individual heats per mole of ligand injected were plotted against the antibiotic/protein molar ratio and the binding parameters were obtained by nonlinear regression of the data (Origin 5.0 software) using, in every case, the simplest model able to describe the protein titration.

The binding of kanamycin-A to wild-type ANT(4′) represents a rather complex process. Thus, the presence of two binding sites per dimer (in region A) plus an additional binding region (herein referred to as B) have been inferred from the structural data available. The ITC curves are consistent with the presence of two high affinity, nonequivalent binding sites per dimer plus an additional site/s characterized by medium-low association constants (K_b) that might reflect nonspecific binding of kanamycin-A to site B (because of the relatively low affinity, its stoichiometry was fixed to a value of 1). For mutant-1, the binding curves can be analyzed assuming two equivalent, high-affinity sites per dimer (~1.8 kanamycin/enzyme stoichiometry) plus an additional site of very low affinity. The alternative analysis of mutant-1 titration in terms of three sequential sites yields two high affinity sites with similar enthalpies of binding and association constants varying in the range expected for equivalent sites,[30] followed by a very low affinity site. Any models simpler than these failed to fit satisfactorily the experimental data. On the other hand, the stoichiometry of 1.8 found for tight complexation of kanamycin-A to mutant-1 supports the assumption of one equivalent per class of site made by sequential binding models. As above, and because of the relatively low affinity, the stoichiometry for kanamycin-A binding to mutant-2 was fixed to a value of 1.

Molecular Mechanics Calculations. Kanamycin-A glycosidic torsion angles were defined as Φ H1−I/C1−I/O1−I/C4−II, and Ψ C1−I/O1−I/C4−II/H4−II for the I/II linkage and Φ H1−III/C1−III/O1−III/C6−II, and Ψ C1−III/O1−III/C6−II/H6−II for the III/II linkage. Relaxed potential energy maps were calculated employing both the AMBER* and MM3* forcefields as implemented in Macromodel.[38] For the III/II fragment of the antibiotic a single orientation for both the glucose hydroxymethyl group (gt, $\omega_{O5-C5-C6-O6} = 60°$) and the secondary hydroxyl groups was considered. Given the unusual structure exhibited by the antibiotic I/II linkage in the crystallographic complex ANT(4′)/kanamycin-A/AMPCPP, a more detailed analysis of its conformational preferences was performed. Thus, in this case, both gt ($\omega_{O5-C5-C6-O6} = 60°$) and tg ($\omega_{O5-C5-C6-O6} = 180°$, as observed in the X-ray structure of the antibiotic/enzyme complex) orientations of the glucose lateral chain were considered. In addition, the starting position for the secondary hydroxyl groups was set as R (reverse clockwise) or C (clockwise) for both rings I and II, rendering four stable combinations, herein referred as RR, RC, CR, and CC. The first character corresponds to the glucose ring while the second one belongs to the 2-deoxy streptamine moiety. Therefore, eight initial configurations were taken into account, and eight different relaxed energy maps were built (see Figures S3 and S4). The previous step involved the generation of the corresponding rigid residue maps by using a grid step of 18°. Then, every point of this map was optimized using 500 steepest descent steps, followed by 5000 conjugate gradient iterations. A dielectric constant $\epsilon = 80$ was employed in all cases. Following this protocol, the rms derivative in low energy regions was smaller than 0.001.

NMR Experiments. The NMR spectra of aminoglycosides **1**−**10** were assigned employing a combination of 2D-TOCSY, NOESY, and HSQC experiments.

The TOCSY,[39] NOESY,[40] and DQF-COSY[41] experiments were performed in the phase-sensitive mode with the TPPI method[41] for quadrature detection in F1. Typically, a data matrix of 2K × 512 points was employed to digitize a spectral width of 4000 Hz. A total of 48 scans were used per increment with a relaxation delay of 1 s. Prior to Fourier transformation, zero filling was performed in F1 to expand the data to 2K × 2K. Baseline correction was applied in both dimensions. The TOCSY spectra were recorded using MLEV-17[39] during the 60 ms of isotropic mixing period. The NOESY experiments were performed with mixing times of 400, 800, and 1000 ms.

HSQC experiments were carried out to obtain the complete ^{1}H and ^{13}C assignment. A data matrix of 1K × 1K was used to digitize a spectral width of 4000 Hz in F_2 and 15000 Hz in F_1; 32 scans were used per increment with a relaxation delay of 1 s and a delay corresponding to a J value of 145 Hz. ^{13}C decoupling was achieved by the WALTZ scheme.

trNOESY experiments were recorded on a Bruker Avance 600 spectrometer, equipped with a cryoprobe, at 303 K. Samples were prepared in D_2O, 10 mM phosphate buffer at pH 7.5–7.8. The concentrations of the different ANT(4′) variants were in all cases, in the 90–100 μM range (monomer concentration). Several ligand/protein ratios from 5:1 to 100:1 were tested for the analysis of both the binary and the ternary complexes. Typically, mixing times from 25 to 400 ms were used. To carry out the experiments with Mg^{2+} ions, 2 to 20 mM $MgCl_2$ were added to the same samples and the pH was readjusted after the addition. For the analysis of the ternary complexes stochiometric amounts of the nucleotide (ATP or AMPCPP) and the ion (Ca^{2+} or Mg^{2+}) were employed. The apparent cross-relaxation rates were derived employing the following protocol. First, trNOE intensities were normalized with respect to the diagonal peak at zero mixing time. Selective T1 measurements were performed on the anomeric protons to get the above-mentioned value. Experimental NOEs were fitted to a double exponential function, $f(t) = p0(e^{-p1t})(1 - e^{-p2t})$ with $p0$, $p1$, and $p2$ being adjustable parameters.[25b] Apparent cross-relaxation rates were determined from the first derivative at time $t = 0$, $f'(0) = p0p2$. The experimental ratios between the structurally relevant cross relaxation rates and those corresponding to the known fixed distances, H1−I/H2−I and H1−III/H2−III, for units I and III, respectively (2.4 Å both), were taken as a first indication of the antibiotic protein-bound geometry.

A theoretical treatment of the trNOE intensities was performed to evaluate the influence of the spin diffusion on the measured cross-peaks and determine the precise geometry of the aminoglycoside in the protein-bound state. Simulations of the trNOE build-up curves were performed employing CORCEMA.[34] Thus the crystallographic coordinates of the ANT(4′)/kanamycin-A (**1**)/AMPCPP ternary complex were employed as starting point. To reduce the dimensions of the matrixes, only nonexchangeable protein protons within a distance of 6 Å to ligand protons were considered in the calculation. First, the kinetic parameters for the free/bound exchange process were estimated by fitting the NOE build-up curves for the intraresidue H1/H2 NOEs (corresponding to a fixed distance of 2.40 Å) in units I and III. In general, a reasonable agreement between experimental and theoretical data was obtained employing τ_c(free) = 0.2 ns, τ_c(bound) = 60–70 ns, $K_a = 10^5$ M^{-1}, $k_{-1} = 300$ s^{-1} for the kanamycin-A/mutant-1 binary complex and $k_{-1} = 50$–75 s^{-1}

(38) Mohamadi, F.; Richards, N. G. J.; Guida, W. C.; Liskamp, R.; Caufield, C.; Chang, G.; Hendrickson, T.; Still, W. C. *J. Comput. Chem.* **1990**, *11*, 440–467.

(39) Bax, A.; Davis, D. G. *J. Magn. Reson.* **1985**, *65*, 355–360.

(40) Kumar, A.; Ernst, R. R.; Wuthrich, K. *Biochem. Biophys. Res. Commun.* **1980**, *95*, 1–6.

(41) Marion, D.; Wuthrich, K. *Biochem. Biophys. Res. Commun.* **1983**, *113*, 967–974.

for the ternary complexes. As a second step, key interresidue trNOEs were calculated employing the previously obtained kinetic parameters. This analysis allows discarding the X-ray geometry as the protein-bound conformation of kanamycin-A in solution. Then minimum energy geometries of the antibiotic, syn-Ψ and anti-Ψ (according to AMBER*, $\epsilon = 80$),[38] were tested. Finally different geometries, close to the minima were also considered until an optimal agreement between the theoretical and experimental trNOEs was obtained.

Enzymatic Activity: NMR Assays. Enzymatic reactions were performed in NMR tubes. The nucleoside triphosphate (ATP 8.0 mM) and the aminoglycoside (1–2 mM) were dissolved in 10 mM phosphate buffer, pH 7.5, 8.0–10.0 mM $MgCl_2$. After addition of the enzyme variants (0.2–20 μM), the evolution of the reaction mixture at 308 K was monitored by 1D ^{1}H NMR, and the final products were characterized by 2D NMR and MALDI-TOF MS.

Enzymatic Activity: HPLC Assays. The formation of the product (AMP-aminoglycoside, retention time = 3.0 min) was followed by HPLC using at Vydac 30I column at 260 nm. The mobile phase was TFA at pH 3.0, and the flow was 1.0 mL min^{-1}. Assay mixtures contained 20 mM sodium phosphate, pH 7.5, 5 mM $MgCl_2$, 3 mM ATP, and variable concentrations of aminoglycoside (0.03–3 mM). The reaction was started by the addition of 0.5 μM of enzyme. Kinetics parameters were derived using built-in nonlinear regression tools within SigmaPlot 8.0. For the determination of apparent kinetic constants, initial velocities (V_i) were fitted to the Michaelis–Menten equation.

Acknowledgment. Financial support from DGES (grants CTQ2004-04494/BQU, CTQ2007-67403/BQU, and CTQ2004-03523/BQU) is acknowledged. J.R. and F.C. thank the Ministerio de Educación y Ciencia for *Juan de la Cierva* and *Ramon y Cajal* contracts, respectively. We also thank CESGA (Santiago de Compostela) for computer support. T.V. thanks CSIC for a JAE contract.

Supporting Information Available: Figures S1 to S21 showing details of the kanamycin-A molecular mechanics calculations, CD, ITC, and kinetic experiments performed with mutants 1–3 together with the NMR characterization of aminoglycosides **1**, **2**, **6**, **7**, **9**, **10**. This material is available free of charge via the Internet at http://pubs.acs.org.

JA076835S